Composition and Vertical Flux of Particulate Organic Matter to the Oxygen Minimum Zone of the Central Baltic Sea: Impact of a sporadic North Sea Inflow

Carolina Cisternas-Novoa[1]*, Frédéric A.C. Le Moigne[1,2], Anja Engel[1].

[1] *GEOMAR, Helmholtz Centre for Ocean Research Kiel, Düsternbrooker Weg 20, D-24105 Kiel*

[2] *Present address:* "Mediterranean Institute of Oceanography, UM 110, Aix Marseille Univ., Université 6 de Toulon, CNRS, IRD, 13288, Marseille, France"

**Corresponding author:* Carolina Cisternas-Novoa, GEOMAR, Helmholtz Centre for Ocean Research Kiel, Düsternbrooker Weg 20, D-24105 Kiel, Germany, +49 431 600-4146 ccisternas@geomar.de

Keywords: Baltic Sea, Oxygen minimum zone, POC, PN, POP, TEP, CSP, Sediment trap, Export efficiency.

Abstract

Particle sinking is a major form to transport photosynthetically fixed carbon to below the euphotic zone via the biological carbon pump (BCP). Oxygen (O_2) depletion may improve the efficiency of the BCP. However, the mechanisms by which O_2 -deficiency can enhance particulate organic matter (POM) vertical fluxes are not well understood. Here, we investigate the composition and vertical fluxes of POM in two deep basins of the Baltic Sea (GB: Gotland basin and LD: Landsort Deep). The two basins showed different O_2 regimes resulting from the intrusion of oxygen-rich water from the North Sea that ventilated the water column below 140 m in GB, but not in LD during the time of sampling. In June 2015, we deployed surface-tethered drifting sediment traps in oxic surface waters (GB: 40 and 60 m; LD: 40 and 55m), within the oxygen minimum zone (OMZ, GB: 110 m and LD: 110 and 180 m), and at recently oxygenated waters by the North Sea inflow in GB (180 m). The primary objective of this study was to test the hypothesis that the different O_2 conditions in the water column of GB and LD affected the composition and vertical flux of sinking particles, and caused differences in export efficiency between those two basins. Composition and vertical flux of sinking particles were different in GB and LD. In GB, particulate organic carbon (POC) flux was 18% lower in the shallowest trap (40 m) than in the deepest sediment trap (at 180 m). Particulate nitrogen (PN) and Coomassie stainable particles (CSP) fluxes decreased with depth, while particulate organic phosphorus (POP), biogenic silicate (BSi), chlorophyll *a* (Chl *a*), and transparent exopolymeric particles (TEP) fluxes peaked within the core of the OMZ (110 m); this coincided with the presence of manganese oxide (MnOx)-like particles aggregated with organic matter. In LD, vertical fluxes of POC, PN, and CSP decreased by 28, 42 and 56% respectively, from the surface to deep waters. POP, BSi and TEP fluxes did not decrease continuously with depth, but they were higher at 110 m. Although we observe higher vertical flux of POP, BSi and TEP coinciding with abundant MnOx-like particles at 110 m in both basins, the peak in the vertical flux of POM and MnOx-like particles was much higher in GB than in LD. Sinking particles were remarkably enriched in BSi, indicating that diatoms were preferentially included in sinking aggregates and/or there was an inclusion of lithogenic Si

(scavenged into sinking particles) in our analysis. During this study, the POC transfer efficiency (POC flux at 180 m over 40 m) was higher in GB (115%) than in LD (69%) suggesting that under anoxic conditions a smaller portion of the POC exported below the euphotic zone was transferred to 180 m than under re-oxygenated conditions present in GB. In addition, the vertical fluxes of MnOx-like particles were two orders of magnitude higher in GB than at LD. Our results suggest that POM aggregates with MnOx-like particles formed after the inflow of oxygen-rich water into GB, the formation of those MnOx-OM rich particles may alter the composition and vertical flux of POM, potentially contributing to a higher transfer efficiency of POC in GB. This idea is consistent with observations of fresher and less degraded organic matter in deep waters of GB than LD.

1. Introduction

Particle sinking is the primary mechanism for transporting photosynthetically fixed carbon below the euphotic zone via the biological carbon pump (BCP) (Boyd and Trull, 2007; Turner, 2015). Previous studies suggested that the transfer of particulate organic carbon (POC) from the euphotic zone to the ocean interior is enhanced in oxygen minimum zones (OMZs) (Cavan et al., 2017; Devol and Hartnett, 2001; Engel et al., 2017; Keil et al., 2016; Van Mooy et al., 2002). Possible mechanisms explaining the higher POC transfer include: i) the reduction of aggregate fragmentation due to the lower zooplankton abundance within the OMZ (Cavan et al., 2017; Keil et al., 2016); ii) the potentially high contribution of refractory terrestrial organic matter (OM) to the POC flux (Keil et al., 2016; Van Mooy et al., 2002); iii) a decrease in heterotrophic microbial activity due to oxygen (O_2) limitation (Devol and Hartnett, 2001); iv) the preferential degradation of nitrogen-rich organic compounds (Kalvelage et al. 2013; Van Mooy et al. 2002, Engel et al. 2017), and v) changes in ballast materials that may alter the sinking velocity and protect OM from degradation (Armstrong et al., 2002). Currently, the study of POC vertical flux in OMZ's has been mostly focused on the tropical ocean (Cavan et al., 2017; Devol and Hartnett, 2001; Engel et al., 2017; Keil et al., 2016; Van Mooy et al., 2002); whereas, how low O_2 concentration would

affect the composition and fate of sinking OM, and the efficiency of the BCP in oxygen-deficient zones of temperate-boreal regimes such as the Baltic deep basins has been less studied.

The semi-enclosed, brackish Baltic Sea is a unique environment with strong natural gradients of salinity and temperature (Kullenberg and Jacobsen, 1981), primary productivity, nutrients (Andersen et al., 2017), and O_2 concentrations (Carstensen et al., 2014a). New production, defined as the fraction of the autotrophic production supported by allochthonous sources of nitrogen (Dugdale and Goering, 1967) is considered equivalent to the particulate OM export (Eppley and Peterson, 1979; Legendre and Gosselin, 1989) on appropriate timescales. In the Baltic Sea, new production varies seasonally (Thomas and Schneider, 1999); with periods of high new production during spring and summer, supported by the diatom-dominated spring bloom and by diazotrophic cyanobacteria respectively (Wasmund and Uhlig, 2003). Based on sediment trap data, collected at 140 m depth in the Gotland Basin (GB), Struck et al. (2004) reported that the highest fluxes of POC occurred in fall, followed by summer and spring. Using $\delta^{15}N$, they showed that during the summer, N_2 fixation by diazotrophic species is the primary source (~41%) of the exported nitrogen and that the majority of the sedimentary particulate organic matter (POM) in the central Baltic Sea is of pelagic origin.

OM export from the euphotic zone to the seafloor has a dual significance in the deep basins of the Baltic Sea. On the one hand, it contributes to the long-term burial of POC, and consequently to the removal and long-term storage of CO_2 from surface waters (Emeis et al., 2000; Leipe et al., 2011), and on the other hand, it connects the pelagic and the benthic systems contributing to the O_2 consumption and hence deoxygenation at depth. Environmental and anthropogenic changes may alter the magnitude and composition of OM transferred from the surface to the seafloor in the Baltic Sea (Tamelander et al. 2017). The reduction of nutrient inputs as targeted by the Baltic Marine Environment Protection Commission (HELCOM) may reduce the OM downward flux and limit the oxygen depletion at depth. However, since hypoxia occurred naturally in the Baltic Sea due to physical processes, mitigating eutrophication will only decrease the spatial extent and intensity of the O2 deficiency in the deep basins.

GB (248 m) and Landsort Deep (LD, 460 m) are the deepest basins of the Baltic Sea. They exhibit permanent bottom-water hypoxia (Conley et al. 2002), caused by a combination of limited water exchange with the North Sea through the Kattegat, strong vertical stratification, and high production /remineralization of OM due to eutrophication (Carstensen et al., 2014b; Conley et al., 2009). A permanent transition zone of about 2 to 10 m thickness separates the oxygenated surface and the oxygen-deficient waters, with a pelagic redoxcline located approximately between 127 and 129 m in GB, and between 79 and 85 m in LD (Glockzin et al., 2014). From the1950s to 1970s, the hypoxic zones (<60 μM) in the Baltic Sea had expanded fourfold (Carstensen et al. 2014). Salt-water inflows from the North Sea are the primary mechanism renewing deep water in the central Baltic Sea (Günter et al., 2008). A Major Baltic Inflow (MBI) occurred in 2014/2015 (Mohrholz et al. 2015); this event ventilated bottom waters for five months between February and July 2015 (Holtermann et al., 2017). This MBI caused the intrusion of O_2 to deep hypoxic waters, substantial temperature variability (Holtermann et al., 2017), displacement of remnant stagnant water masses by new water that changed the chemistry of the water column (Myllykangas et al., 2017), and high turbidities that may be associated with redox reactions products (Schmale et al., 2016). At the time of sampling (June 2015), the MBI had reached GB but did not affect LD, located further northwest. The oxygenated water inflow reached GB at the beginning of March and created a secondary near-bottom redoxcline (Schmale et al., 2016); the bottom water anoxia started to re-established in July 2015 (Dellwig et al., 2018). In LD, water properties did not change due to the MBI, the sulfidic layer was maintained (hydrogen sulfide, H_2S concentrations of 20.7- 21.2 μM), and salinity varied between 10.6 and 10.9 (Holtermann et al., 2017).

Pelagic redoxclines are the suboxic transition between oxic and anoxic - even sulfidic- waters. A steep redox gradient characterizes this transition zone were electron acceptors and their reduced counterparts are vertically segregated, and biogeochemical transformations mediated by microbial processes are actively occurring (Bonaglia et al., 2016; Brettar and Rheinheimer, 1991; Neretin et al., 2003). For instance, iron (Fe) and manganese (Mn) undergo rapidly reversible transformations at the redox interface. Mn is an essential electron donor and acceptor in redox processes occurring

at brackish, pelagic systems with anoxic conditions like the deep basins of the Baltic Sea. Redox conditions control the biogeochemical transformations between dissolved Mn^{2+} and insoluble oxides and hydroxides of Mn^{4+}. Under anoxic conditions dissolved reduced Mn forms dominate, while in the presence of O_2 the formation of particulate manganese oxides (MnOx) is favored. The concentration of dissolved Mn may reach 0.3 μM in GB and a maximum value of about 3 μM in the LD (Dellwig et al., 2012). Van Hulten et al. (2017) estimated an aggregation threshold for manganese oxides of 25 pM, and suggested that a minimal concentration of dissolved Mn is required for an efficient aggregation and removal of MnOx. Therefore, in GB and LD, the balance between dissolve Mn and the formation of MnOx is controlled by the O_2 availability (*e.g.*, Neretin et al., 2003). LD is characterized by a permanently stratified water column and sulfidic bottom waters; these conditions favored the accumulation of high concentrations of dissolved Mn (Dellwig et al., 2012).

In contrast, GB is periodically affected by lateral intrusions of O_2 and the oxygenation of deep water as a result of MBI that occur every one to four years (Matthäus and Franck, 1992), favoring the occurrence of MnOx containing particles. MnOx production may be microbially mediated (Richardson et al., 1988), or authigenic (Glockzin et al., 2014). In sulfidic waters, the reduction of MnOx with sulfide occurs within a scale of seconds to minutes (Neretin et al., 2003), and is inhibited by nitrate (Dollhopf et al., 2000). The oxygenation of the deep water of GB by the 2014/2015 MBI combined with the release of Mn from the sediments into the water column (Lenz et al., 2015) generate appropriate conditions to enhance particulate MnOx formation and vertically expand the zone where they could be observed in the water column.

MnOx-containing particles have previously been observed at pelagic redoxclines in the Baltic Sea (Glockzin et al., 2014; Neretin et al., 2003). They are amorphous or star-shaped particles, and occur as single particles or form aggregates with OM (Neretin et al., 2003), specifically with transparent exopolymer particles (TEP) (Glockzin et al., 2014). The sinking velocity (0.76 m d^{-1}) of those mixed aggregates containing MnOx and TEP was lower than what was predicted by Stokes law possibly due to their star-shaped morphology and the high OM content. TEP are

highly sticky, polysaccharide-rich particles that can enhance particle aggregation rates and the formation of marine snow (Engel, 2000; Logan et al., 1995). Thus, the sinking of MnOx-OM aggregates may contribute to the downward flux of POC. However, high content of TEP relative to more dense particles could reduce the density of marine aggregates and decrease their sinking velocity (Engel and Schartau, 1999). Another type of less studied exopolymer particles are Coomassie stainable particles (CSP), they are protein-containing particles that stain with Coomassie brilliant blue (Long and Azam 1996). Little is known about the characteristics and dynamics of those particles in marine systems and their potential to form aggregates with MnOx had not been studied. Different to TEP, CSP have a limited role on the aggregation of diatoms (Prieto et al., 2002; Cisternas-Novoa et al., 2015), but seem to be important for the aggregation of cyanobacteria (Cisternas-Novoa et al., 2015). Mixed MnOx-OM aggregates may affect the cycling of particle-reactive elements like phosphorus and trace metals via scavenging processes, and it has been proposed that they could act as carriers of bacteria in the redoxcline (Dellwig et al., 2010). To date, there are no measurements of the density of MnOx-OM aggregates, their potential ballast effect on sinking OM, or their biogeochemical role modifying the vertical flux of POM in the Baltic Sea.

The objectives of this study are, first, to determine the amount and composition of particles sinking out of the euphotic zone into the deep basins of the Baltic Sea: GB and LD. Second, to study how the oxygenation of deep waters (>140 m) caused by the 2014/2015 MBI may affect the vertical flux of sinking particles. We, therefore, compared GB affected by the MBI with LD that was not affected and exhibited low O_2 concentration (>74 m) and even sulfidic conditions (>180 m). We hypothesized that the MBI that altered the water column chemistry and created different O_2 conditions in GB compared with LD affected the composition and vertical flux of sinking particles. Additionally, the higher abundance and *in-situ* formation of MnOx-OM aggregates may cause differences in degradation and export of OM between those two basins.

2. Methods

2.1. Sampling location and water column properties

Samples were collected during the BalticOM cruise in the Baltic Sea onboard the *RV Alkor* form June 3th to June 19th, 2015. We collected sinking particles using surface-tethered drifting sediment traps (Engel et al., 2017; Knauer et al., 1979) in GB and LD (Table 1). Additionally, water column samples (table 2) were collected using a Niskin-bottle rosette at the locations of the trap deployments. Temperature, salinity and O_2 concentration were determined at each station using a Sea-Bird (CTD) probe equipped with a O_2 sensor (Oxyguard, PreSens), calibrated with discrete samples measured using the Winkler method (Strickland and Parsons, 1968; Wilhelm, 1888).

2.2. Sediment trap design and deployment

We deployed two surface-tethered drifting sediment traps for two days in GB, and one day in LD (Fig.1). Each trap collected particles at four depths: 40 m (two arrays were deployed to evaluate replicability of particle collection), 60 m (55m in LD), 110 m and 180 m (Table 1) to estimate POM fluxes to and within the OMZ. 40 m was considered as the base of the euphotic zone based on PAR measurements conducted during the cruise (data not shown). At each depth, 12 acrylic particle interceptor tubes (PITs) mounted in a PVC cross frame were deployed. Each PIT was equipped with an acrylic baffle at the top to minimize the collection of swimmers (Engel et al., 2017; Knauer et al., 1979). The PITs were 7 cm in diameter and 53 cm in height with an aspect ratio of 7.5 and a collection area of 0.0038 m^{-2}. The cross frame and PITs were attached to a line that had a bottom weight and a set of surface and subsurface floats. The procedures for PIT preparation and sample recovery followed Engel et al. (2017). Shortly before deployment, each PIT was filled with 1.5 L of seawater previously filtered through a 0.2 μm pore size cartridge. A preservative solution of saline brine (50 g L^{-1}) was added slowly to each PIT underneath the 1.5 L of filtered seawater, carefully keeping the density gradient. The PITs were kept covered until deployment and immediately after recovery to avoid contamination. After recovery, the density gradient was visually verified, and the supernatant seawater was siphoned off the PIT. Then, we pooled together the remaining water, containing the sinking material (~0.6-0.8 L), of 12 tubes per depth into a large container, that we filled-up to 10 L with filtered seawater (between 0.4 and 1.5 L) to have the same volume per depth. After that, the samples were screened with a 500 μm mesh

to remove swimmers (Conte et al., 2001). Subsequently, samples were split into aliquots that were processed for the different biogeochemical analysis as described in Engel et al. (2017).

2.3. Biogeochemical analysis

Nutrients were measured in seawater samples collected in the deployment stations. Ammonium (detection limit of 0.05 µM) was measured directly on unfiltered seawater samples on board after Solórzano (1969). Phosphate, nitrate, and nitrite (detection limit of 0.04 µM) were filtered through a 0.2 µm pore size and stored frozen until their analysis; samples were measured photometrically with continuous flow analysis on an auto-analyzer (QuAAtro; Seal Analytical) after Grasshoff et al. (1999).

Particulate organic carbon (POC), nitrogen (PN), organic phosphorus (POP), and chlorophyll *a* (Chl *a*) were determined as described in Engel et al. (2017). Aliquots, of 100 to 200 mL of the trapped material and 500 mL of the seawater samples, were filtered in duplicate for each parameter at low vacuum (<200 mbar), onto pre-combusted GF/F filters (8h at 500°C). The filters were stored frozen (-20°C) until analysis. Prior analysis, filters for POC-PN determination were exposed to acid fumes (37% hydrochloric acid) to remove carbonates and subsequently dried for 12h at 60 °C. POC and PN concentrations were determined using an elemental analyzer (Euro EA, Hechatech) after Sharp (1974).

POP was analyzed after Hansen and Koroleff (1999). POP was oxidized to orthophosphate by heating the filters in 40 mL of deionized water (18.2MΩ) with Oxisolv (MERCK 112936) for 30 min in a pressure cooker. Orthophosphate was determined spectrophotometrically at 882 nm in a Shimadzu UV-VIS Spectrophotometer UV1201.

Chl *a* was analyzed after extraction with 10 mL of 90% acetone, the fluorescence of the samples was measured using a Turner fluorometer (440/685 nm, Turner, 10-AU) according to Strickland et al. (1972). The fluorometer was calibrated with a standard solution of Chl *a* (Sigma-Aldrich C-5753).

Biogenic silica (BSi) was determined in aliquots of 50 to 100 mL, filtered in duplicate onto 0.4 µm cellulose acetate filters. Samples were stored at -20°C until analysis. For the measurements,

filters were digested in NaOH at 85°C for 135 min; the pH was adjusted to 8 with HCl. Silicate was measured spectrophotometrically according to Hansen and Koroleff (2007).

Polysaccharide (TEP) and protein (CSP) exopolymer particles, from sediment trap and water column samples were analyzed by microscopy according to Engel (2009). Duplicate aliquots of 5 to 20 mL were filtered onto 0.4 μm Nuclepore membrane filters (Whatmann) and stained with 1 mL of Alcian Blue solution, a dye that target acidic polysaccharides, for TEP or 1 mL of Coomassie brilliant blue solution, a dye commonly used to stain proteins (Bradford, 1976), for CSP. Filters were transferred onto Cytoclear ® slides and frozen (-20°C) until microscopy analysis. For the analysis, thirty images for each filter were captured under 200x magnification using a light microscope (Zeiss Axio Scope A.1) connected to a color camera (AxioCam MRc). Particle abundance and area were measured semi-automatically using an image analysis system including the WCIF ImageJ software. The RGB was split into three channels: red, blue and green, and the red was used to quantify the amount of TEP and CSP. Additionally, TEP and CSP in water samples from the stations where we deployed sediment traps were analyzed spectrophotometrically (with higher vertical resolution than microscopy) according to Passow and Alldredge (1995) and Cisternas-Novoa et al. (2014), respectively. Concentrations of TEP are reported relative to a xanthan gum standard and expressed in micrograms of xanthan gum equivalents per liter (μg XG eq. L^{-1}), and concentrations of CSP are reported relative to a bovine serum albumin standard and expressed in micrograms of bovine serum albumin equivalents per liter (μg BSA eq. L^{-1}).

MnOx-containing particles have been commonly identified based on their morphology, size and elemental composition, confirmed by scanning electron microscopy (SEM) and energy dispersive x-ray microanalysis (EDX) (Neretin et al., 2003; Glockzin et al., 2014; Dellwig et al., 2010, 2018). In this study, we did not measure the elemental composition of the particles. Thus, we identified them as "MnOx-like particles" based on similar morphology, size, and association with organic matter (OM) as MnOx-containing particles previously described in the Baltic Sea (eg., Neretin et al., 2003 and Glockzin et al., 2014). The abundance and size of MnOx-like particles

were determined using particle recognition on filters and imaging processing similar to the method used by Neretin et al. (2003) but without the chemical composition analysis of the particles. For the image analysis, we used the same images as for TEP and CSP analysis and modified image analysis procedure described above as follows: thirty images per filter (200x) were analyzed semi-automatically using ImageJ software. After RGB split, the blue channel pictures were used to quantify MnOx-like particles in the water column and sediment traps. In this manner, the MnOx-like particles were clearly visible with a negligible disruption from TEP or CSP stained blue.

Total hydrolyzable amino acids (TAA) were analyzed in unfiltered seawater and trapped material. Samples were stored at -20°C until analysis. Duplicate samples were hydrolyzed at 100 °C in 6N HCl (Suprapur® Hydrochloric acid 30%) and 11 mM ascorbic acid for 20h. Amino acids were separated and measured by high-performance liquid chromatography (HPLC), after derivatization with ortho-phthaldialdehyde using a fluorescence detector (Excitation/Emission 330/445 nm) (Dittmar et al., 2009; Lindroth and Mopper, 1979). TAA concentrations were reported as µM of monomer. The quantitative degradation index (DI) of Dauwe et al. (1999), based on changes in amino acids composition of POM as it undergoes degradation processes, was calculated using the factor coefficient of Dauwe et al. (1999) and the average and standard deviation of the TAA of this data set.

Total combined carbohydrates (TCHO) > 1 kDa were determined by HPAEC-PAD according to Engel and Händel (2011). TCHO were analyzed in the unfiltered seawater and sediment trap material. Samples were stored at -20°C until analysis. Prior to analysis, the samples were desalted by membrane dialysis using dialysis tubes with 1 kDa molecular weight cut-off (Spectra Por). Desalination was conducted for 4.5h at 1°C. Then, a 2 mL subsample was sealed with 1.6 mL of 1M HCl in pre-combusted glass ampoules and hydrolyzed for 20h at 100°C. After hydrolysis, the subsamples were neutralized by acid evaporation under N_2 atmosphere at 50°C, resuspended with ultrapure Milli-Q water and analyzed on a Dionex 3000 ion chromatography system. TCHO concentrations were reported as µM of monomer.

2.4 Phytoplankton abundance

Phytoplankton composition and abundance at the stations where we deployed sediment traps were evaluated using light microscopy and flow cytometry. Counts of phytoplankton cells > 5 μm, were made from 50 mL of fixed samples (Lugol's solution, 1% final concentration). Samples were concentrated using gravitational settling and counted under a Zeiss Axiovert inverted microscope (200x magnification) following the guidelines for determination of phytoplankton species composition, abundance (HELCOM, 2012). The counts were made on either half (cyanobacteria, diatoms, and *Dinophysis sp*.) or two strips (chryptophyta, unidentified dinoflagellates, and chlorophyta) of the chamber. Individual filaments of cyanobacteria were counted in 50 μm length units. The size of the counted phytoplankton species ranged from 10 to 200 μm.

Phytoplankton, <20 μm, cell abundance was quantified using a flow cytometer (FACSCalibur, Becton, Dickson, Oxford, UK). 2 mL samples were fixed with formaldehyde (1% final concentration) and stored frozen (-80 °C) until analysis (two weeks later). Red and orange autofluorescence were used to identify chlorophyll and phycoerythrin cells. Cell counts were determined with CellQuest software (Becton Dickenson); pico- and nanoplankton populations of naturally containing chlorophyll and/or phycoerythrin (*i.e.*, Synechococcus) were identified and enumerated.

2.5 Statistics

Significant differences between two parameters were tested using the Mann-Whitney U-test. The results of statistical analyses were assumed to be significant at *p*-values < 0.05. Statistical analyses were performed using Matlab software (MatlabR2014a).

3. Results

3.1. Biogeochemistry of the water column

At both stations, GB and LD, the water column was stratified during the study. In GB, the seasonal thermocline was located between 22 and 37 m, with temperature decreasing rapidly from 9.8°C in the surface mix layer to 4.7°C below 37 m (Fig. 2a). Deeper in the water column, a pycnocline (halocline) coincided with the oxycline and was located between 65 m (S=7.6) and 80 m (S=10.2); below 80 m the salinity gradually increased up to 13.5 (220 m). A hypoxic layer (<40

μM O_2) was located between 74 and 140 m; the core of the OMZ (<10 μM O_2) was located between 96 and 125 m. The O_2 concentration increased from 35 μM O_2 at 140 m to 79 μM O_2 at 220 m (Fig. 2a). In LD, the seasonal thermocline was located between 10 and 39 m, where the temperature decreased gradually from 12°C to 4.0°C (Fig. 2b). The pycnocline was between 55 (S=7.2) and 75 m (S=9) below that the salinity was constant (S=10.7) until the bottom of the station (430 m). The O_2 concentration was below the detection limit (<3 μM O_2) from 74 m to the deepest point sampled in LD (430 m).

The vertical profile of nutrients was different at both stations (Fig. 2). In GB, nitrate concentration increased from below the detection limit in the upper ten meters to 0.17 μM at 40 m (Fig. 2a). Concentrations were variable within the OMZ with 6 μM in the upper (80 m) and lower oxycline (140 m), and 0.12 μM in the core of the OMZ (110 m). Nitrate concentration was 4.8 μM in the deepest sample (220 m). Nitrite was below the detection limit in most of the water column except for 60 m (0.09 μM) and 110 m (0.11 μM). Ammonium increased from 0.14 μM in the upper ten meters to 1.15 μM at 40 m; concentrations were variable within the OMZ with less than 0.15 μM in the upper (80 m) and lower oxycline (140 m), and maximum concentration of 3.28 μM in the core of the OMZ (110m). Vertical profiles of phosphate and silicate at GB were similar; the concentrations steadily increased from the upper ten meters of the water column (0.29 μM and 10.36 μM, respectively) to the OMZ (2.67 μM and 39.07 μM, respectively), and gradually decreased below the OMZ (Fig. 2a). H_2S was not detectable in GB.

In LD, nitrate and nitrite concentrations were below the detection limit between the surface and 250 m (<0.04 μM) (Fig. 2b). Nitrite showed a maximum of 0.22 μM at 350 m, and nitrate a maximum of 6.0 μM at 400 m. Ammonium concentrations varied between 0.06 and 0.59 μM in the upper 70 m and increased to 5.97 and 8.03 μM in the OMZ (>74 m). The lowest ammonium concentration (0.07μM) was measured in the surface and the highest (8.03 μM) at 110 m. Phosphate and silicate concentrations were relatively low within the mixed layer; gradually increased below the pycnocline, and decreased again between 110 and 180 m. Phosphate concentrations varied between 1.5 and 2.5 μM in the upper 110 m of the water column, decreased

to 0.22 μM at 180 m and increased to 2.7 μM at 430 m (deepest sample). Silicate ranged between 25 and 38 μM in the upper 110 m of the water column, decreased to 7.4 μM at 180 m, and increased to 38.9 μM at 430 m. H_2S was detectable below 180 m, with the highest concentration (3.97 μM) at 250 m and the lowest (0.04 μM) between 300 and 350 m (Fig. 2b).

3.2. Particulate organic matter concentration in the water column

Chl *a* concentration in the upper 10 m was slightly higher in GB (1.5-1.7 μg L^{-1}, Fig. 3b) than in LD (1.4-1.2 μg L^{-1}, Fig. 3e). At both stations, more than 90% of the total smaller phytoplankton (<20 μm, pico- and nanophytoplankton) abundance, determined by flow cytometry, were measured in the upper 60 m, although phytoplankton was detectable in the entire water column. Pico- and nanophytoplankton abundance were 10% higher in GB than in LD (Table 2). Picocyanobacteria determined by phycoerythrin fluorescence accounted for 92% and 96% of the total picophytoplankton abundance in GB and LD, respectively. Picocyanobacteria abundance was 30% higher in GB than in LD.

Phytoplankton (>5 μm) abundance, determined by microscopy, was 63% higher in LD than in GB (Table 3). Filamentous cyanobacteria dominated the phytoplankton community at both stations with up to 90% corresponding to *Aphanizomenon* sp. Cyanobacteria represented 56% of the phytoplankton counts in GB and up to 74% in LD. Dinoflagellates (including mixotrophs), dominated by *Dinophysis* sp, were significant in both stations (19% of the phytoplankton counts), whereas chlorophytes (dominated by filaments of *Planctonema* sp. containing cylindrical cells) were more abundant in GB than in LD (25% and 4% of the phytoplankton counts respectively). Diatoms represented less than 1% of the phytoplankton in both stations, and they were slightly more abundant at 40 m in LD (Table 3). BSi was higher in the upper 10 m (0.4-0.5 μM) and decreased with depth in GB (Fig. 3b), whereas in LD, BSi showed a peak at 40 m and then decreased with depth (Fig. 3e).

Vertical profiles of POC, PN, and POP concentration were similar in the water column of the two stations (Fig. 3a, d). In GB, the concentrations were higher in the upper 10 m of the water column (POC: 40.38 ± 0.80, PN: 3.89± 0.01, and POP: 0.26± 0.04 μM) and decreased gradually with

depth until 110 m where relatively high concentrations (POC 18 ± 0.63, PN: 2± 0.08, and POP: 0.2 μM) were observed. The lowest concentrations were found at 180 m (POC: 11.97 ± 1.03, PN: 1.05± 0.02, and POP <0.03 μM) (Fig. 3a). In LD, POM decreased with depth from the surface (POC: 35 ± 0.99, PN: 4± 0.09, and POP: 0.2 μM) to 40 m, remained relatively constant between 40 and 80 m and decreased again between 110 and 250 m (Fig. 3d).

We observed high concentrations of TEP and CSP in the upper 10 m in both stations. The highest TEP concentration was determined at 1 and 10 m at both stations, and it was slightly higher (19%) in GB than in LD (Fig. 3c, f). TEP and CSP vertical profiles were different from each other in GB (Fig. 3c) and covaried in LD (Fig. 3f). Like observed for POC, PN, and POP, TEP concentrations showed a peak at 110 m (50.29± 6.17 μg XG eq. L^{-1}) in GB. The highest concentration of CSP at this station was observed in the shallowest (1 m) sample, CSP concentration decreased quickly below 10 m, and then it increased at 140 and 220 m (the deepest sample, approximately 28 m above the seafloor) (Fig. 3c). In LD, the highest concentrations of TEP and CSP were measured at the surface (1 and 10 m) and at 110 m (Fig. 3f). TEP and CSP decreased with depth in the first 80 m (from 53.26± 7.10 to 18.39± 4.57 μg XG eq. L^{-1} and from 53.26± 7.10 to 31.57± 18.78 μg BSA eq. L^{-1}). Both types of gel-like particles showed an increase in concentration at 110 m (49.25± 4.08 μg XG eq. L^{-1} and 66.89± 22.33 μg BSA eq. L^{-1} respectively). Below 110 m, TEP concentrations stayed relatively constant, while CSP concentrations decreased at 180 m and kept relatively constant below that depth.

3.3. MnOx-like particles vertical distribution in the water column

Dark, star-shaped MnOx-like particles (Glockzin et al., 2014; Neretin et al., 2003) were only observed below the fully oxygenated mixed layer in GB and, in less abundance, in LD (Fig. 4). In GB, MnOx-like particles were observed from 80 m to 220 m; they appear as single particles and forming large aggregates containing several MnOx-like particles associated with OM. Relatively high concentration of MnOx-like particles ($2x10^6$ particles L^{-1}) were observed in the upper (80 m, 25 μM O_2) and lower (140 m, 36 μM O_2) oxycline, and at 220 m, 79 μM O_2 ($4x10^6$ particles L^{-1})(Fig. 4a). The lowest abundance of MnOx-like particles ($7x10^5$ particles L^{-1}) was observed at

110 m, 6 μM O_2, i.e. in the core of the OMZ. The equivalent spherical diameter (ESD) of MnOx-like particles varied between 0.6 and 30.5 μm, with a median size of 3.0 μm. The largest aggregates (up to 30.5 μm) were observed in the upper oxycline (80 m). In LD, MnOx-like particles were less abundant, smaller, and had a narrow distribution in the water column than in GB. MnOx-like particles were not detected in the fully oxic (0-40 m) or fully anoxic (180 to 430 m) water column. At 60 m (135 μM O_2), right above the oxycline, MnOx-like particles began to appear, however, in relatively low abundance. The maximum abundance of MnOx-like particles, $9x10^5$ L^{-1}, was observed in the oxycline at 70 m (27 μM O_2, Fig. 4b). The ESD ranged between 0.6 and 13.4 μm, the largest aggregates were observed at 70 m.

3.4. Vertical flux of Sinking Particles

Vertical fluxes of POC and PN varied little with depth in GB (Fig. 5a). POC flux slightly increased by 18% from the shallowest (40 m) to the deepest (180 m) sediment trap. Fluxes of PN (Fig. 5a) and CSP (Fig. 6b) were higher at 40 and 60 m and decreased (19 and 70 %) from 60 to 180 m respectively. On the other hand, fluxes of POP, BSi, Chl *a* (Fig. 5b) and TEP (Fig. 6a) peaked in the sediment trap located in the core of the OMZ (110 m). The increment of fluxes at 110 m coincided with the high abundance of MnOx-like particles associated with TEP (Fig. 6a). In addition, TEP size distribution, determined by image analysis, indicated an increase in large TEP at 110 m (data not shown). In contrast, in LD, POC, PN (Fig. 5c) and CSP (Fig. 6d) fluxes, steadily decreased with depth by 28, 42 and 56% from 40 to 180 m. Similar to the fluxes measured in GB, the POP, BSi (Fig. 5d) and TEP (Fig. 6c) showed a smaller peak in the sediment trap located at 110 m.

MnOx-like particles were drastically less abundant in sediment trap samples from LD than in GB, and when present, they appeared as single particles, not aggregated with TEP or CSP (Fig. 6c, d). At both stations, and similar to the water column samples, MnOx-like particles were not observed in sediment trap samples collected in fully oxygenated waters (40 and 60 m). The flux of MnOx-like particles at 110 and 180 m was two orders of magnitude larger in GB than in LD (Table 4). In GB, MnOx-like particles occurred as single particles as well as aggregates with each other and

OM such as TEP and CSP (Figure 6a,b, and e), phytoplankton cells, or detrital material. The ESD of MnOx-like particles and aggregates collected in the traps ranged from 0.6 to 167 μm (median 2.8 μm) at 110 m and from 0.6 to 153 μm (median 3.3 μm) at 180 m. In LD, only a few, single MnOx-like particles were observed at 110 m (Fig. 6 c, d), their size ranged from 0.6 to 16.5 mm (median 1.8) (Table 4).

TAA flux ranged from 371±12 to 501± 33 μmol $m^{-2}d^{-1}$ in GB and from 502± 84 to 785± 54 μmol $m^{-2}d^{-1}$ in LD (Fig. 7a). In GB, the flux steadily decreased from surface to depth, whereas in LD the TAA flux at 40 m was lower than at 60 m and decreased with depth from 60 to 180 m (Fig. 7b). The vertical profile of TCHO flux was similar in both stations, although the magnitude of the flux was higher at LD. The TCHO flux varied between 303± 8 and 428± 14 μmol $m^{-2}d^{-1}$ in GB (Fig. 7a) and between 503± 19 and 584± 8 μmol $m^{-2}d^{-1}$ in LD (Fig. 7b). At both stations, TCHO fluxes increased from 40 to 110 m, where the highest flux was measured, and then it decreased at 180 m.

3.5. *Chemical composition of sinking and suspended particles*

Comparing molar elemental ratios of sinking (from sediment trap material) and suspended (from water column) particles to the revisited Redfield ratio for living plankton (106C: 16N: 15Si: P; Redfield et al., 1963; Brzezinski, 1985), our results showed that the POC:PN ratio of sinking particles was slightly above this ratio at both stations. The POC:PN ratios of sinking particles in GB and LD were not significantly different. In GB however, ratios increased with depth from 9.8 to 12.6, while in LD it varied between 11.1 and 15.4 without a clear trend with depth. The POC:POP ratio of sinking particles was lower ($p<0.05$; Mann–Whitney U-test) in GB (90.1-244) than in LD (230-772) with the highest value observed at 40 m and the lowest at 110 m. At both stations the POC:BSi ratios varied between 1.7 and 4.2 and PN:BSi ratios varied between 0.2 and 0.4; the lowest values were observed at 110 m (Table 5).

Contrastingly, in suspended particles, POC:PN ratios were higher in GB than in LD ($p<0.001$). In GB, it varied between 8.4 and 12 without a clear trend with depth; while in LD, it decreased with depth from 8.7 (at 1m) to 6.2 (at 400 m), and a slightly higher value of 7.8 was observed at 430 m.

The POC:PN and POC:POP were significantly higher ($p<0.01$) in sinking than in suspended particles (Table 5). The POC:BSi and the PN:BSi ratios were much lower in sinking than in suspended particles at both stations (GB: $p<0.05$; LD: $p<0.01$). In sinking particles, the POC:BSi ratio was below Redfield ratio of 7, whereas it was one to two orders of magnitude higher in suspended particles (Table 5). The PN:POP ratio was significantly lower in sinking (0.15-0.43) than in suspended particles (9.7-44.5) at both stations ($p<0.001$). In sinking particles, it was always below the Redfield ratio of 16, while in suspended particles, it was in the range of Redfield ratio in the upper 80 m in GB and always above in LD.

At both stations, the contribution of AA to POC was more significant in sinking than in suspended particles. Similarly, the carbon contained in TCHO made up a larger percentage in sinking than in suspended particles (Table 5). The amino acid-based degradation index (DI, Dauwe et al., 1999) varied from 0.1 to 1.14 in sinking OM and was higher than in suspended OM (-1.25 to -0.42) in both stations. In sinking OM, the DI decreased with depth in GB, whereas in LD, there was not a clear trend with depth (Table 5). The DI was higher in GB than in LD in sinking as well as in suspended OM.

4. Discussion

In this study, we 1) characterized the biogeochemistry of the water column and the sinking particles in GB and LD, during early summer 2015, and 2) determined the vertical flux of sinking particles in those two deep basins of the Baltic Sea. Our results suggested that the intrusion of oxygenated water to GB, as consequence of the 2014/2015 MBI, caused changes in the water chemistry that affected the chemical composition and degradation stage of the sinking and suspended particles. Consequently, the composition and magnitude of the sinking particle flux were different in GB and LD.

4.1 Physical and biogeochemical conditions in GB and LD

In general, physical and biogeochemical conditions (temperature, salinity, O_2, and inorganic nutrient concentrations) were similar in the euphotic zone of both stations. Moreover, though there were slight differences between the stations concerning phytoplankton abundance and

composition, and concentration and chemical composition of POM, in the surface water column, those were not significant. The concentration of Chl *a* (Fig. 3) and the abundance of pico- and nano-phytoplankton (Table 2) were slightly higher (20 and 10 % respectively) in GB than in LD. This agrees with estimates of integrated total primary production (PP), which were 10% higher in GB (380 mg C m^{-2} d^{-1}) than in LD (334 mg C m^{-2} d^{-1}; Piontek et al., unpublished). At both stations, the abundance of pico-phytoplankton (<2 μm) was an order of magnitude higher than nano-plankton (Table 2). These findings coincided with what was described previously for early summer in the Baltic Sea that indicate that during this period the productivity is sustained mostly by pico- and nano-phytoplankton communities (Leppänen et al., 1995) which co-existed with cyanobacteria and other phytoplankton species (Kreus et al. 2015). Microscopic analysis, on the other hand, indicated that phytoplankton (>5 μm) abundance was 47% higher in LD than in GB. At both stations, filamentous cyanobacteria (> 90% *Aphanizomenon* sp.) were numerically the predominant phytoplankton type (55 and 74% of the phytoplankton counts in GB and LD respectively), dinoflagellates (including mixotrophs) correspond to 20%, and diatoms correspond to >1% of the phytoplankton abundance in the upper 40 m (Table 3). Diatoms were slightly higher in LD than in GB, and this coincided with a small peak in BSi concentration (1.5 μM, Fig. 3e) at 40 m in LD. Although at both stations the diatom proportion from the total phytoplankton abundance was negligible, they could make a difference in the composition of sinking particles leaving the euphotic zone in LD due to selective aggregation of diatoms (Passow et al., 1991); however, in both stations sinking particles showed a similar enrichment in BSi. The low abundance of diatoms relative to cyanobacteria in the euphotic zone indicated that at both stations, the spring bloom was terminated and cyanobacteria were starting to build up the summer bloom that generally occurs in June-July (Kreus et al., 2015); *Aphanizomenon* sp. and *Nodularia spumigena*, are known to form summer blooms, where they accumulate at the sea surface of the thermally stratified water column (Bianchi et al., 2000; Nausch et al., 2009; Wasmund, 1997).

The concentration of particulate elements (POC, PN, POP, BSi) was slightly higher in the surface waters of GB compared to LD; while polysaccharide (TEP) and protein (CSP) containing

exopolymeric particles were in similar abundance at both stations. TEP and CSP were more abundant in the euphotic zone, which supports the idea of a phytoplankton origin; however, the concentration of TEP in this study was 69% (in GB) and 76% (in LD) lower than previously reported for summer in the central Baltic Sea (Engel et al., 2002). Likewise, our dissolved inorganic nitrogen concentrations were below the detection limit in the surface, while phosphate concentrations were higher (>0.3 μM) than observed in the Engel et al. (2002) study. Mari and Burd (1998) reported that TEP concentration peaked during the spring bloom and in summer in the Kattegat. TEP production may be enhanced by environmental conditions such as nutrient limitation (Mari et al., 2005; Passow, 2002), which are characteristic of late summer in the Baltic Sea (Mari and Burd 1998). In the Baltic Sea, the spring bloom (March-April) is usually followed by a period of reduced PP (Chl-*a* ~ 2 μgL^{-1}) that precedes the cyanobacteria summer bloom, typically observed in June-July (Kreus et at., 2015). Surface satellite-derived Chl-*a* concentrations (MODIS) in GB constantly increase from mid-May to mid-June 2015 (Le Moigne et al., 2017); our monthly Chl-*a* concentrations derived from VIIRS for June 2015 in the Baltic Sea (Fig.1) showed similar Chl-*a* concentrations. Considering this trend in Chl-*a* concentration and the availability of phosphate in the water column, we could assume that our samples were collected at the beginning of the summer bloom (middle June). In general ecosystem models from the Baltic Sea indicate that the termination of the summer bloom depends upon phosphate availability (Kreus et at., 2015). Thus, likely TEP concentrations had not reached the higher value previously observed after the summer bloom when inorganic nutrients were depleted. Although satellite-derived Chl-*a* concentrations is a valuable tool to evaluate the trend of the PP, the magnitude of the concentration of Chl-*a* from remote sensing is difficult to estimate in the Baltic Sea (Darecki and Stramski, 2004). The concentration of Chl-*a* in GB and LD derived from direct measurements were much lower (~1.5 $\mu g\ L^{-1}$), suggesting that our samples were collected during a period of low phytoplankton biomass typically observed before the summer bloom. In any case, the concentration of phosphate was not limiting the system. Another possible explanation for the rather low concentrations of TEP could be their removal from the surface by aggregation and

subsequent sedimentation during the spring bloom due to the high abundance of cells and detrital particles during this time (Engel et al., 2002) and the relatively low grazing pressure that lead to higher export after the spring bloom (Lignell et al., 1993).

Although the composition and amount of OM in the surface waters at the two trap stations were similar, below the euphotic zone (40 m) the vertical profile of nutrients and particulate matter concentrations were distinctly different; likely due to the 2014/2015 MBI (Holtermann et al., 2017) that reached the deep waters of GB. This inflow replaced the old stagnant water masses by new water masses (Schmale et al., 2016), changing the salinity in the deepest waters and the vertical distribution of O_2 increasing its concentrations below140 m and constraining the oxygen-deficient layers from 74 to 140 m depth. The combination of physical effects (the displacement of water masses, turbulent mixing and lateral transport) and the consequent development of redox conditions through 2015 may have impacted the distribution of MnOx-like particles and POM in GB. In addition to changes in O_2 concentration, the MBI altered the redox conditions in GB creating a secondary redoxcline at 140 m, where concentrations of O_2 and MnOx-like particles increased. One consequence of those changes is the vertical extension of the layer in which MnOx-containing aggregates could form (Schmale et al., 2016); a previous study showed that MnOx might precipitate from the water column of GB following a MBI event (Lenz et al., 2015). POC and PN concentrations peaked at 110 m, this higher concentration at 110 m was even more evident in POP and TEP, while CSP concentration peaked at 140 m (Fig. 3); this is the first study that examines the potential role of CSP in forming aggregates with MnOx-containing particles. The highest concentration of MnO-like particles (Fig. 4a) in the water column was not observed at 110 m (the core of the OMZ) but at 80 m (oxycline), and below 140 m in the newly oxygenated water layers.

In contrast, LD maintained permanent suboxic (<5 μM O_2) waters below 74 m as H_2S was detectable below 180 m. Below 100 m the vertical profiles of POM and BSi did not change with depth. The only exception was TEP and CSP concentration that similar to in GB peaked at 110 m and MnOx- like particles showed a small increment at 70 m (in the oxycline). This suggest that,

similar to the results of Glockzin et al (2014), the MnOx-like particles, abundant in the oxycline may form sinking aggregates with TEP and CSP, then, when those aggregates sunk to anoxic waters (below 74 m), the MnOx-like particles may dissolve releasing TEP and CSP to the water column, where CSP concentration decreased quickly likely due to microbial degradation, but the concentration of TEP remain constant to the bottom of LD.

MBI can have a significant impact on nutrient recycling. In GB nitrate concentration increased possibly as a consequence of the oxidation of reduced nitrogen compounds (e.g., ammonium, ammonia and organic nitrogen compounds like urea) (Le Moigne et al., 2017) that accumulated during the stagnation (anoxic) period previous to the MBI (Hannig et al., 2007). Scavenging of phosphate onto Mn or Fe oxides has been shown in previous studies (Neretin et al., 2003). Phosphate can bind to Fe hydroxides and MnOx and settle down during oxic conditions, building up a phosphate pool in the sediments that later on when the O_2 decreases may become a source of phosphate (Gustafsson and Stigebrandt, 2007). Moreover, Myllykangas et al. (2017) reported that the new water masses intruded during 2014/2015 MBI displaced the stagnant water masses in GB. Thus, the low concentrations of silicate and phosphate that we measured in the deep waters of GB may also be a direct consequence of the intrusion of oxygenated, low-nutrient waters associated with the MBI. In contrast, in LD, the water column remained anoxic down to the sea floor (430 m), below the oxycline an increase of ammonium was observed (Fig.2b), which could be an indicator for anaerobic respiration of OM, e.g., denitrification (Bonaglia et al., 2016; Hietanen et al., 2012).

In summary, though GB and LD had similar surface conditions in terms of phytoplankton production and POM stocks, during this study, we found differences in the vertical concentration of nutrients (Fig. 2) and POM (Fig. 3) between GB, ventilated by the MBI, and LD, a station that remained suboxic. Our results suggest that the MBI caused differences in the vertical profile of O_2 that modified the redox conditions of the water column and enhance the *in-situ* formation of MnOx-like particles (Fig. 4). Alternatively, the inflow may transport new MnOx-like particles to

GB. Those abundant MnOx-like particles may aggregate with POM in GB, influencing the vertical distribution of POM in the water column.

4.2 Potential influence of O_2 concentration and redox conditions on vertical flux of sinking particles in GB and LD

During this study, we also investigated the effect of different O_2 concentrations and redox conditions on the fluxes of particles. Our measurement of POC flux at 40 m, below the euphotic zone, were 11.7±0.82 mmol C m^{-2} d^{-1} in GB and 19.8±1.22 mmol C m^{-2} d^{-1} in LD. Extrapolating those measurements to annual flux, we obtain 4.37±0.31 mol C m^{-2} yr^{-1} in GB and 7.44±0.46 mol C m^{-2} yr^{-1} in LD. Our results from GB are in the same range as the estimation derived from a biogeochemical model; *i.e.* 3.8 - 4.2 mol C m^{-2} yr^{-1} (Kreus et al., 2015; Sandberg et al., 2000; Stigebrandt, 1991) for the Baltic Sea; however, our results from LD are higher than the annual POC fluxes predicted by those models. The high POC flux observed in this study is not surprising since it represented one (in LD) and two (in GB) days in June when the POC vertical flux out of the euphotic zone is relatively high in the Baltic Sea compared with late fall and winter. The biogeochemical model of Kreus et al. (personal communication) estimated that POC flux in June ranged between 8 and 13 mmol $m^{-2}d^{-1}$; this is in the same range that our observations.

One of the main advantages of our sediment traps is that we can study the flux of sinking particles at various depths simultaneously (i.e. higher vertical resolution). Therefore, we measured the POM flux in oxic waters (40 m and 60 (55) m); at the core of the OMZ (110 m) at 180 m in both basins. Traps located a 180 m depth collected particles in sulfidic waters at LD and in recently oxygenated waters (affected by the MBI) in GB. The vertical flux of POM and BSi was different at the two studied basins; for example, POC flux was between 25 and 40% higher in the upper 110 m of the LD than in GB (even though the PP was 10% higher in GB). However, the POC fluxes at 180 m (deepest trap) weresimilar in both basins; indicating a substantial decrease in the POC flux between 110 and 180 m at the LD. The POC flux (and the PN flux which showed a similar vertical profile) did not decrease with depth in the GB. In contrast, in the LD there was a

reduction of 17 and 16% of the POC flux from 40 m and 60 m (in the oxycline) and from 110 to 180 m respectively; the POC flux did not change from 60 to 110 m when a large section of the water column was suboxic (O_2 < 5 μM from 74 m to the bottom of the station). From 110 to 180 m the water column was completely anoxic, and H_2S was detectable at 180 m. The high flux of POC at GB coincided with the appearance of dark, star-shaped particles that we defined as MnOx-like particles, particularly evident at GB (Fig. 6a,b, and e), but also present in LD. Based on their morphology, size, and aggregation with OM, we propose that those particles correspond to MnOx-containing particles enriched in OM that have been previously described at GB (Neretin et al., 2003; Pohl et al., 2004; Glockzin et al., 2014; Dellwig et al., 2010, 2018) and LD (Glockzin et al., 2014; Dellwig et al., 2010). The higher flux of MnOx-like particles in GB than in LD is probably due to the oxygenation and changes in the deep water redox conditions that enhance the formation of MnOx-like particles associated with OM. This suggests that the reduction of the POC flux below 110 m in the LD may be related to the O_2 depletion and the absence of MnOx-OM aggregates in the anoxic zone.

The POP flux was similar in the oxic water column (up to 60 m) in both basins; however, it was almost two and three times higher at 110 and 180 m respectively in GB than in LD. A peak in the POP and BSi flux was observed at 110 m in both basins, but the magnitude of the increment was much higher GB than in LD. In GB the POP flux increased 62% from 60 to 110 m (OMZ) and then decreased by 28% from 110 to 180 m. Vertical flux of POP, BSi, and Chl-*a* (Fig. 5) were enhanced at 110 m, which coincided with the high flux of MnOx-like particles. This high flux of MnOx-like particles is maintained at 180 m, while the POP, BSi and Chl-*a* flux decreased at this depth. This vertical distribution is is likely due to the enhanced formation of MnOx-like particles in the hypoxic layer (<40 μM O_2) located between 74 and 140 m that may scavenge POP, and aggregate with cells or phytodetritus containing BSi and Chl-*a*. Although the POP flux peaked at 110 m in LD as well, the increment was only 30 % from 60 m (suboxic) to 110 m (anoxic), and it decreased by 78% from 110 to 180 m (sulfidic waters), these variations with depth were also

observed in the BSi flux. In LD, the flux and size of MnOx-like particles were much smaller than in GB, and they were more abundant at 110 m than at 180 m.

Similar to the vertical distribution of POM in the water column discussed in section 4.1, differences in POM and BSi fluxes between basins are likely associated with the large inflow of oxygen-rich saltwater that displaced the old-stagnant water masses and changed the chemistry of the water column (Myllykangas et al., 2017). Under euxinic conditions (*e.i.*, scenario observed in LD without the influence of the MBI), the maximum concentration of particulate Mn is found in the oxycline (Glockzin et al., 2014). Below the oxycline, and due to the presence of H_2S, the particulate Mn concentration decreased drastically. During this study, we observed a high concentration of MnOx-like particles flux at 110 and 180 m (Table 5) in GB, in agreement with the high flux of particulate Mn measured in sediment traps located at 186 m in June 2015 (Dellwig et al., 2018). The oxygenation of the deep water layers of GB by the MBI caused the absence of H_2S (Schmale et al., 2016) and provided redox conditions favorable for the formation of MnOx, resulting in the high MnOx-like particles flux measured in the sediment trap located in the core of the OMZ (110 m) and at 180 m (oxygenated deep water). There were two possible sources of MnOx associated with the 2014/2015 MBI in GB. On the one hand, the lateral transport of low-density aggregates formed by MnOx and OM (Glockzin et al., 2014), and on the other hand, the *in-situ* formation and deposition of MnOx following the oxygenation of the water column (Dellwig et al., 2018). In clear contrast to the oxygenated deep layers of GB, in LD, we measured H_2S below 180 m, this could explain why although those aggregates were present in this station at 110 m, they may dissolve in sulfidic waters, thus, were not as abundant and did not form aggregates with TEP (Fig.6c).

The presence of MnOx-like particles in aggregates (Fig 6a) may have implications for the vertical flux of POC, PN and POP in a stratified system with a pelagic redoxcline like the Baltic Sea. Under steady state, the upward diffusion and oxidation rates of the dissolved Mn are balanced by the sinking and dissolution rates of MnOx. During Mn-oxidation, the MnOx could aggregate with POM and trace metals. Then, in the sulfidic waters, slow-sinking MnOx enriched in OM will be

dissolved liberating the OM and altering the vertical distribution and the flux of all associated particle elements (Glockzin et al., 2014). This has been previously observed in other anoxic basins; for example, in the Cariaco Basin, total particulate phosphorus reached their maximum flux in sediment traps close to the redoxcline (Benitez-Nelson et al., 2004; Benitez-Nelson et al., 2007). Moreover, even in the anoxic zone, the abundant aggregate associated bacteria (Grossart et al., 2006) could partially or entirely degrade the organic compounds in those particles using NO_3^- or MnOx as an electron acceptor. This may explain why we observed a clear peak in the vertical fluxes of POP, BSi, Chl-*a* (Fig. 3a, b), TEP (Fig. 6a) and TCHO (Fig. 7a) at 110 m, followed by a small decrease at 180 m in GB. In LD a smaller increment in the vertical fluxes of POP, BSi (Fig. 3d), TEP (Fig. 6c) and TCHO (Fig. 7b) were also observed. The vertical fluxes of those compounds coincided with the abundance of MnOx-like particles; we assume that the MnOx aggregated not only with TEP as described before (Glockzin et al. 2014) and observed in this study (Fig. 6a), but also with aggregates containing phytoplankton cells and phytodetritus that may enhance POP, BSi, Chl *a*, and TCHO export. On the other hand, nitrogen-rich components of POM like PN (Fig. 3a), TAA (Fig. 7a), and CSP (Fig. 6a) gradually decreased with depth in GB, suggesting that those compounds were less scavenge by MnOx-OM rich aggregates.

Primary production (PP) in GB was 10% higher than in LD during our study (Piontek et al. unpublished data). However, the POC flux below the euphotic zone (at 40 m) was 42% higher in LD than in GB and comparable at both stations at 180 m. The fraction of PP exported as POC is termed export production (*e-ratio*) (Buesseler et al., 1992), and it is calculated as the POC flux below the euphotic zone divided by the PP. We calculated the *e-ratio* using ^{14}C-based PP measurements (Piontek et al. unpublished data) and carbon flux at 40 m (shallowest sediment trap depth, considered at the base of the euphotic zone). The *e-ratio* was larger in LD (0.77) compared to GB (0.41)*; i.e.*, the percentage of the PP exported as POC below the euphotic zone was 77% in LD versus 41% in GB. This suggests that either a higher proportion of the PP was remineralized in the euphotic zone of GB compared with LD, or particles were sinking faster in LD than in GB likely due to differences in composition. On the other hand, the transfer efficiency of POC to the

deeper water column (*i.e.*, the ratio of POC flux at180 m over POC flux at 40 m) was higher in GB (115%) than in LD (69%). The transfer efficiency of POM is largely controlled by the remineralization rate and the sinking velocity of particles (De La Rocha and Passow, 2007; McDonnell et al., 2015; Trull et al., 2008). The higher POC transfer efficiency in GB than in LD can be attributable to differences in the sinking velocities of the particles in those two stations. Particulate MnOx may sink through the redoxcline in GB (Neretin et al., 2003) acting as ballast material and nucleus for MnOx-OM rich aggregates formation. Those aggregates could have sunk more quickly, limiting the time spent in the water column and the degradation by particle-attached microbes. Assuming that MnOx-like particles had a density between 1.5 and 2.0 g cm^{-3} (Glockzin et al., 2014), the largest particles measured at GB (167 μm, Table 4) will have a sinking velocity based on Stokes' law between 508 and 1014 m d^{-1}. If we consider a mixed aggregate that is 50% TEP, density 0.9 g cm^{-3} (Azetsu-Scott and Passow, 2004) and 50% MnOx (density 1.5 g cm^{-3}), its density would be 1.2 g cm^{-3}, and its theoretical sinking velocity will be 204 m d^{-1}. This indicates that, theoretically, the largest mixed aggregates composed of MnOx and TEP observed in GB could reach 180 m (the location of our deepest sediment trap) in less than one day. However, the average measured sinking velocity of MnOx-containing particles in the laboratory for particles between 2 and 20 μm was 0.76 m d^{-1}, which is significantly lower than the theoretical value (Glockzin et al., 2014). Glockzin et al. (2014) suggested that the star shape and the content of OM were responsible for the lower than predicted sinking velocity. There is no information about the amount of OM relatively to MnOx-containing particles in those mixed aggregates, or how the MnOx to OM ratio may affect the density and sinking velocity of larger aggregates like the ones we observed. Due to the shape and size of MnOx-OM aggregates observed in our study (Fig. 6e), we could assume those are the same type of aggregates described before by Glockzin et al. (2014). Although we did not measure the sinking velocity of those aggregates, we did observe a higher abundance of them associated with TEP at 110 and 180 m in GB than in LD. Thus, the formation of MnOx aggregates rich in OM could represent an additional mechanism (see introduction) to explain why the efficiency of the OM export is different under anoxic than under

oxic conditions in the Baltic Sea. The oxygenation of anoxic deep water in GB caused by the 2014/2015 MBI, may have led to enhanced precipitation of manganese, iron, and phosphorus particles (Dellwig et al., 2010; Dellwig et al., 2018). For example, the formation of P-rich, metal oxides precipitates occur in the anoxic waters of the Black Sea (Shaffer, 1986) and Cariaco Basin (Benitez-Nelson et al., 2004; Benitez-Nelson et al., 2007) were higher concentration of particulate inorganic and organic phosphorus have been observed in sediment traps close to the redoxcline.

Alternatively, BSi could also act as ballast material incrementing the sinking velocity of marine aggregates (Armstrong et al., 2001; Klaas and Archer, 2002). Our results showed that sinking particles were strongly enriched in BSi relatively to C and N and compared to suspended particles that were depleted in BSi (Table 5). Diatoms are the major phytoplankton group that produces BSi to build their cell walls (Martin-Jézéquel et al., 2000), and they are the dominant phytoplankton species during the spring bloom. However, during our study, diatoms represented less than 1% of the phytoplankton abundance in the water column, and even though there was a strong enrichment in BSi in the sinking particles, this was similar in GB and LD (Table 5). Therefore, either the differences in export production nor in transfer efficiency between GB and LD could not be solely explained by the amount of diatoms cells, phytodetritus or BSi in sinking particles at those two basins.

4.3 Differences on composition and lability of sinking and suspended organic matter in GB and LD

In the sections above we compared the biogeochemical conditions and the size of the POM pool in the euphotic zone of GB and LD. We then looked at how the sinking flux of OM was affected by the different O_2 concentrations in the water column. Now, we focus on the influence of O_2 in the chemical composition of sinking and suspended particles. Suspended or slow sinking particles that spend more time in the water column should theoretically, show a more substantial degree of degradation (Goutx et al., 2007). Relative to the Redfield molar ratio: 106 POC:16 PN:15 BSi: POP. POM showed enrichment in POC relative to PN and POP, especially in sinking particles

from LD and suspended particles from GB. Our measured values of POC:PN (~10) and POC:POP (between 89 and 506) in suspended OM coincide with the simulated ratio reported immediately after the culmination of the spring bloom by Kreus et al. (2015). The same study had suggested that POC:POP higher than Redfield ratio might lead to an enhancement of particle export (Kreus et al., 2015), however, no direct observations had confirmed this hypothesis. Our measurements showed that the relative higher POC:POP ratios in sinking OM from LD, compared with GB, do not lead to a higher transfer efficiency at this station. Compared to the suspended OM in LD, the POP content was lower in GB, possible related to scavenging of POP into MnOx aggregates (see section 3.4).

In addition, at both stations, sinking particles were strongly enriched in BSi (Table 5) probably due to the preferential sinking of diatoms and remnants diatom-rich detritus from the spring bloom. Differently, suspended particles had a relatively low content of BSi; this is not surprising considering the small proportions of diatoms in the euphotic zone at the time of our sampling. The concentration of BSi decreased below the detection limit from 60 m in the GB, and 70 m in the LD. This observation coincides with previous studies reporting selective incorporation of diatoms into sinking aggregates in the Baltic Sea (Engel et al., 2002; Passow, 1991), whereas non-diatoms species, although they may be abundant in the suspended phytoplankton, may not be present in sinking particles (Passow, 1991).

Another explanation for of higher BSi content in sinking particles may be the inclusion of lithogenic Si in our measurements; lithogenic Si may have been present in the water column or being transported by laterally adverted material. A recent study suggests that contributions of non-biogenic sources could be significant during alkaline extraction (Barão et al., 2015). The even more substantial enrichment in BSi observed in sinking particles from 110 m in both basins, may result from adsorption and/or co-precipitation of silica in sinking particles containing MnOx (Dellwig et al., 2010; Hartmann, 1985); or by the formation of aggregates that are enriched in MnOx as well as in phytodetritus from diatom origin.

The TAA based degradation index, DI (Dauwe et al. 1999) covers a wide range of alteration stages; the more negative the DI, the more degraded the samples, positive DI indicates fresh organic matter. In our study, the sediment trap material had a DI between 0.10 and 1.14, while suspended OM has a DI between -0.26 and -1.25 (Table 5). These values coincide with what reported earlier by Dauwe et al. (1999), and indicate that: first, the sinking particles collected in the sediment traps were less altered (they have a more positive DI) than the suspended OM collected in the Niskin bottle. Second, sinking particles from GB were fresher than the ones from LD, and the degradation stage increased with depth in both stations. The higher contribution of AA and CHO to the POC pool in sinking than in suspended OM and the AA- DI indicates that suspended OM was more degraded than sinking OM. The highest degree of degradation in suspended OM and sinking OM from LD may be the result of a long time that light suspended OM or slow sinking particles spend exposed to degradation in fully oxygenated surface waters than dense, fast sinking particles collected in sediment traps.

The higher abundance of aggregates, formed by a combination of MnOx-like particles and OM, observed at 110 and 180 m in GB could act as bacteria hot spots that combined with a higher O_2 concentration in GB may increase the microbial degradation on sinking particles collected in GB. However, the AA-DI, indicated that sinking OM was less altered, and therefore more labile than the sinking OM in LD. This implied that in addition to the higher transfer efficiency of POC in GB (see discussion above); the OM reaching the seafloor was fresher and less degraded. This supports the idea that mix aggregates composed by MnOx and OM may be larger and faster sinking than the previously described by Glockzin et al. (2014). This explanation is mostly speculative, and based on the observation of large mixed aggregates in the 110 and 180 m traps (Fig. 6, Table 4). However, as mention in the previous section, further work on directly determining sinking velocity is required to prove this hypothesis.

Conclusion

Fluxes and composition of sinking particles were different in two deep basins in the Baltic Sea: GB and LD during early summer 2015. The two stations had similar surface characteristics and POM stock; however, at depth, the vertical profile of the POM concentration, as well as the vertical flux of sinking particles was different, likely related to differences in the O_2 concentration. The 2014/2015 MBI supplied oxygen-rich waters to GB transporting solid material from shallower areas and modifying the O_2 vertical profile and the redox conditions in the otherwise permanent suboxic deep waters. This event did not affect LD allowing for the comparison of POM fluxes and composition under two different O_2 concentrations with similar surface water conditions. Export efficiency (*e-ratio*) derived from *in-situ* PP measurements and POC flux derivate from sediment traps indicated higher export efficiency in LD than in GB. However, the transfer efficiency (POC flux at 180 m over POC flux at 40 m) suggested that under anoxic conditions found in LD, a smaller portion of the POC exported below the euphotic zone was transferred to 180 m than under oxygenated conditions present in GB. The MBI also transport solid Mn from shallower areas towards GB deep that may have contributed to the higher abundance of MnOx-OM in GB. Our results suggest that a new possible mechanism to explain the differences in the OM fluxes under different O_2 concentration could be the formation and prevalence of aggregates composed of MnOx and organic matter in GB. Those aggregates were significantly larger and more abundant in GB compared to LD where sulfidic waters constrained their presence. Our results indicate that at GB not only a higher proportion of the POM leaving the euphotic zone reached our deepest sediment trap, but also that this POM was fresher and less degraded. We propose that after a MBI in GB, the aggregates containing MnOx-like particles and organic matter could have reached the sediments relatively fast and unaltered, scavenging not only phosphorus and TEP, as described previously, but also other compounds like BSi, POP and CSP. The higher fraction of sinking particles exported below the euphotic zone and reaching 180 m in GB suggest that at this station a significant fraction of the POM could reach the sediments, 50 m below our deepest sediment trap, relatively unaltered. The remineralization of the organic matter reaching the sediments may contribute to the quick re-establishment of anoxic conditions in the sediment-water interface in GB. The relevance of this process needs to be further

investigated in order to be included in O_2 budget and long-term predictions of the MBI impact in the O_2 and OM cycles.

Author Contributions

C.C.N. designed and performed the sediment trap work at sea, analyzed samples and wrote the manuscript. F.A.C.L.M, designed and performed the sediment trap work at sea and contributed to the writing of the manuscript. A.E designed and participated in the scientific program at sea and discussed and commented on the manuscript.

Acknowledgements

This research was supported by the DFG Collaborative Research Center 754 "Climate-Biogeochemistry Interactions in the Tropical Ocean" (to A.E., C.C.N. and F.A.C.L.M), by a Fellowship of the Excellence Cluster 'The Future Ocean' (CP1403 to F.A.C.L.M.), and by a DAAD short term grant (57130097 to C.C.N.). We thank Jon Roa, Tania Klüver, Scarlett Sett, Angela Stippkugel, Carola Wagner, Clarissa Karthäuser, Moritz Ehrlich, Sonja Endres, Hannes Wagner, Ruth Flerus, Sven Sturm and Christian Begler for support during traps preparation and deployments, help with experiment or analyzed samples. We Thank Judith Piontek for her contribution to the design of the scientific program at sea, Jaime Soto- Neira for valuable discussion and help with figure preparation, Annegret Stuhr for useful discussion about phytoplankton data and Cindy Lee for helpful advice. We gratefully acknowledge the reviewers Monika Nausch and Tom Jilbert, and the associated editor Marcel van der Meer for their time and effort in reviewing and editing the manuscript which significantly improved this publication.**References**

Andersen, J. H., Carstensen, J., Conley, D. J., Dromph, K., Fleming-Lehtinen, V., Gustafsson, B. G., Josefson, A. B., Norkko, A., Villnäs, A., and Murray, C.: Long-term temporal and spatial trends in eutrophication status of the Baltic Sea, Biological Reviews, 92, 135-149, 2017.

Armstrong, R. A., Lee, C., Hedges, J. I., Honjo, S., and Wakeham, S. G.: A new, mechanistic model for organic carbon fluxes in the ocean based on the quantitative association of POC with ballast minerals, Deep Sea Research Part II: Topical Studies in Oceanography, 49, 219-236, 2002.

Azetsu-Scott, K. and Passow, U.: Ascending marine particles: Significance of transparent exopolymer particles (TEP) in the upper ocean, Limnology and Oceanography, 49, 741-748, 2004.

Barão, L., Vandevenne, F., Clymans, W., Frings, P., Ragueneau, O., Meire, P., Conley, D. J., and Struyf, E.: Alkaline-extractable silicon from land to ocean: A challenge for biogenic silicon determination, Limnology and Oceanography: Methods, 13, 329-344, 2015.
Benitez-Nelson, C. R., O'Neill, L., Kolowith, L. C., Pellechia, P., and Thunel, l. R.: Phosphonates and particulate organic phosphorus cycling in an anoxic marine basin, Limnology and Oceanography, 49, 1593-1604, 2004.
Benitez-Nelson, C. R., O'Neill Madden, L. P., Styles, R. M., Thunell, R. C., and Astor, Y.: Inorganic and organic sinking particulate phosphorus fluxes across the oxic/anoxic water column of Cariaco Basin, Venezuela, Marine Chemistry, 105, 90-100, 2007.
Bianchi, T. S., Engelhaupt, E., Westman, P., Andrén, T., Rolff, C., and Elmgren, R.: Cyanobacterial blooms in the Baltic Sea: Natural or human-induced?, Limnology and Oceanography, 45, 716-726, 2000.
Bonaglia, S., Klawonn, I., Brabandere, L. D., Deutsch, B., Thamdrup, B., and Brüchert, V.: Denitrification and DNRA at the Baltic Sea oxic–anoxic interface: Substrate spectrum and kinetics, Limnology and Oceanography, 61, 1900-1915, 2016.
Boyd, P. W. and Trull, T. W.: Understanding the export of biogenic particles in oceanic waters: Is there consensus?, Progress in Oceanography, 72, 276-312, 2007.
Bradford, M. M.: A rapid and sensitive method for the quantitation of microgram quantities of protein utilizing the principle of protein-dye binding, Analytical Biochemistry, 72, 248-254, 1976.
Brettar, I. and Rheinheimer, G.: Denitrification in the Central Baltic: evidence for H ₂ S-oxidation as motor of denitrification at the oxic-anoxic interface, Marine Ecology Progress Series, 77, 157-169, 1991.
Buesseler, K. O., Bacon, M. P., Kirk Cochran, J., and Livingston, H. D.: Carbon and nitrogen export during the JGOFS North Atlantic Bloom experiment estimated from 234Th: 238U disequilibria, Deep Sea Research Part A. Oceanographic Research Papers, 39, 1115-1137, 1992.
Carstensen, J., Andersen, J. H., Gustafsson, B. G., and Conley, D. J.: Deoxygenation of the Baltic Sea during the last century, Proceedings of the National Academy of Sciences, 111, 5628-5633, 2014a.
Carstensen, J., Conley, D. J., Bonsdorff, E., Gustafsson, B. G., Hietanen, S., Janas, U., Jilbert, T., Maximov, A., Norkko, A., Norkko, J., Reed, D. C., Slomp, C. P., Timmermann, K., and Voss, M.: Hypoxia in the Baltic Sea: Biogeochemical Cycles, Benthic Fauna, and Management, AMBIO, 43, 26-36, 2014b.
Cavan, E. L., Trimmer, M., Shelley, F., and Sanders, R.: Remineralization of particulate organic carbon in an ocean oxygen minimum zone, Nature Communications, 8, 14847, 2017.
Cisternas-Novoa, C., Lee, C., and Engel, A.: A semi-quantitative spectrophotometric, dye-binding assay for determination of Coomassie Blue stainable particles, Limnology and Oceanography: Methods, 12, 604-616, 2014.
Conley, D. J., Björck, S., Bonsdorff, E., Carstensen, J., Destouni, G., Gustafsson, B. G., Hietanen, S., Kortekaas, M., Kuosa, H., Markus Meier, H. E., Müller-Karulis, B., Nordberg, K., Norkko, A., Nürnberg, G., Pitkänen, H., Rabalais, N. N., Rosenberg, R., Savchuk, O. P., Slomp, C. P., Voss, M., Wulff, F., and Zillén, L.: Hypoxia-Related Processes in the Baltic Sea, Environmental Science & Technology, 43, 3412-3420, 2009.
Conte, M. H., Ralph, N., and Ross, E. H.: Seasonal and interannual variability in deep ocean particle fluxes at the Oceanic Flux Program (OFP)/Bermuda Atlantic Time Series (BATS) site in the western Sargasso Sea near Bermuda, Deep Sea Research Part II: Topical Studies in Oceanography, 48, 1471-1505, 2001.
Darecki, M. and Stramski, D.: An evaluation of MODIS and SeaWiFS bio-optical algorithms in the Baltic Sea, Remote Sensing of Environment, 89, 326-350, 2004.
Dauwe, B., Middelburg, J. J., Herman, P. M. J., and Heip, C. H. R.: Linking diagenetic alteration of amino acids and bulk organic matter reactivity, Limnology and Oceanography, 44, 1809-1814, 1999.

De La Rocha, C. L. and Passow, U.: Factors influencing the sinking of POC and the efficiency of the biological carbon pump, Deep Sea Research Part II: Topical Studies in Oceanography, 54, 639-658, 2007.
Dellwig, O., Leipe, T., März, C., Glockzin, M., Pollehne, F., Schnetger, B., Yakushev, E. V., Böttcher, M. E., and Brumsack, H.-J.: A new particulate Mn–Fe–P-shuttle at the redoxcline of anoxic basins, Geochimica et Cosmochimica Acta, 74, 7100-7115, 2010.
Dellwig, O., Schnetger, B., Brumsack, H.-J., Grossart, H.-P., and Umlauf, L.: Dissolved reactive manganese at pelagic redoxclines (part II): Hydrodynamic conditions for accumulation, Journal of Marine Systems, 90, 31-41, 2012.
Dellwig, O., Schnetger, B., Meyer, D., Pollehne, F., Häusler, K., and Arz, H. W.: Impact of the Major Baltic Inflow in 2014 on Manganese Cycling in the Gotland Deep (Baltic Sea), Frontiers in Marine Science, 5, 2018.
Devol, A. H. and Hartnett, H. E.: Role of the oxygen-deficient zone in transfer of organic carbon to the deep ocean, Limnology and Oceanography, 46, 1684-1690, 2001.
Dittmar, T., Cherrier, J., and Ludwichowski, K. U.: The analysis of amino acids in seawater. In: Practical guidelines for the analysis of seawater Wurl, O. and Raton, B. (Eds.), CRC Press, 2009.
Dollhopf, M. E., Nealson, K. H., Simon, D. M., and Luther, G. W.: Kinetics of Fe(III) and Mn(IV) reduction by the Black Sea strain of Shewanella putrefaciens using in situ solid state voltammetric Au/Hg electrodes, Marine Chemistry, 70, 171-180, 2000.
Dugdale, R. C. and Goering, J. J.: Uptake Of New And Regenerated Forms Of Nitrogen In Primary Productivity, Limnology and Oceanography, 12, 196-206, 1967.
Emeis, K. C., Struck, U., Leipe, T., Pollehne, F., Kunzendorf, H., and Christiansen, C.: Changes in the C, N, P burial rates in some Baltic Sea sediments over the last 150 years—relevance to P regeneration rates and the phosphorus cycle, Marine Geology, 167, 43-59, 2000.
Engel, A.: The role of transparent exopolymer particles (TEP) in the increase in apparent particle stickiness (α) during the decline of a diatom bloom, Journal of Plankton Research, 22, 485-497, 2000.
Engel, A., Meyerhöfer, M., and von Bröckel, K.: Chemical and Biological Composition of Suspended Particles and Aggregates in the Baltic Sea in Summer (1999), Estuarine, Coastal and Shelf Science, 55, 729-741, 2002.
Engel, A. and Schartau, M.: Influence of transparent exopolymer particles (TEP) on sinking velocity of Nitzschia closterium aggregates, Marine Ecology Progress Series, 182, 69-76, 1999.
Engel, A., Wagner, H., Le Moigne, F. A. C., and Wilson, S. T.: Particle export fluxes to the oxygen minimum zone of the eastern tropical North Atlantic, Biogeosciences, 14, 1825-1838, 2017.
Eppley, R. W. and Peterson, B. J.: Particulate organic matter flux and planktonic new production in the deep ocean, Nature, 282, 677, 1979.
Glockzin, M., Pollehne, F., and Dellwig, O.: Stationary sinking velocity of authigenic manganese oxides at pelagic redoxclines, Marine Chemistry, 160, 67-74, 2014.
Goutx, M., Wakeham, S. G., Lee, C., Duflo, s. M., Guigue, C., Liu, Z., Moriceau, B., Sempére, R., Tedetti, M., and Xue, J.: Composition and degradation of marine particles with different settling velocities in the northwestern Mediterranean Sea, Limnology and Oceanography, 52, 1645-1664, 2007.
Grossart, H. P., KiÃƒÂ¸rboe, T., Tang, K. W., Allgaier, M., Yam, E. M., and Ploug, H.: Interactions between marine snow and heterotrophic bacteria: aggregate formation and microbial dynamics, Aquatic Microbial Ecology, 42, 19-26, 2006.
Gustafsson, B. G. and Stigebrandt, A.: Dynamics of nutrients and oxygen/hydrogen sulfide in the Baltic Sea deep water, Journal of Geophysical Research: Biogeosciences, 112, 2007.
Hannig, M., Lavik, G., Kuypers, M. M. M., Woebken, D., Martens-Habbena, W., and JÜrgens, K.: Shift from denitrification to anammox after inflow events in the central Baltic Sea, Limnology and Oceanography, 52, 1336-1345, 2007.
Hansen, H. P. and Koroleff, F.: Determination of nutrients. In: Methods of Seawater Analysis, Wiley-VCH Verlag GmbH, 2007.

Hansen, H. P. and Koroleff, F.: Determination of nutrients. In: Methods of Seawater Analysis., Grasshoff, K., Kremling, K., and Ehrhardt, M. (Eds.), Willey-VCH, Weinheim, Germany, 1999.
Hartmann, M.: Atlantis-II Deep geothermal brine system. Chemical processes between hydrothermal brines and Red Sea deep water, Marine Geology, 64, 157-177, 1985.
HELCOM: Guidelines for monitoring phytoplankton species composition, abundance and biomass. In: Manual for Marine Monitoring in the COMBINE

Programme of HELCOM, Helsinki Commission, Helsinki 2012.
Hietanen, S., Jäntti, H., Buizert, C., Jürgens, K., Labrenz, M., Voss, M., and Kuparinen, J.: Hypoxia and nitrogen processing in the Baltic Sea water column, Limnology and Oceanography, 57, 325-337, 2012.
Holtermann, P. L., Prien, R., Naumann, M., Mohrholz, V., and Umlauf, L.: Deepwater dynamics and mixing processes during a major inflow event in the central Baltic Sea, Journal of Geophysical Research: Oceans, 122, 6648-6667, 2017.
Keil, R. G., Neibauer, J. A., Biladeau, C., van der Elst, K., and Devol, A. H.: A multiproxy approach to understanding the "enhanced" flux of organic matter through the oxygen-deficient waters of the Arabian Sea, Biogeosciences, 13, 2077-2092, 2016.
Knauer, G. A., Martin, J. H., and Bruland, K. W.: Fluxes of particulate carbon, nitrogen, and phosphorus in the upper water column of the northeast Pacific, Deep Sea Research Part A. Oceanographic Research Papers, 26, 97-108, 1979.
Kreus, M., Schartau, M., Engel, A., Nausch, M., and Voss, M.: Variations in the elemental ratio of organic matter in the central Baltic Sea: Part I—Linking primary production to remineralization, Continental Shelf Research, 100, 25-45, 2015.
Kullenberg, G. and Jacobsen, T. S.: The Baltic Sea: an outline of its physical oceanography, Marine Pollution Bulletin, 12, 183-186, 1981.
Le Moigne, F. A. C., Cisternas-Novoa, C., Piontek, J., Maßmig, M., and Engel, A.: On the effect of low oxygen concentrations on bacterial degradation of sinking particles, Scientific Reports, 7, 16722, 2017.
Legendre, L. and Gosselin, M.: New production and export of organic matter to the deep ocean: Consequences of some recent discoveries, Limnology and Oceanography, 34, 1374-1380, 1989.
Leipe, T., Tauber, F., Vallius, H., Virtasalo, J., Uścinowicz, S., Kowalski, N., Hille, S., Lindgren, S., and Myllyvirta, T.: Particulate organic carbon (POC) in surface sediments of the Baltic Sea, Geo-Marine Letters, 31, 175-188, 2011.
Lenz, C., Jilbert, T., Conley, D. J., Wolthers, M., and Slomp, C. P.: Are recent changes in sediment manganese sequestration in the euxinic basins of the Baltic Sea linked to the expansion of hypoxia?, Biogeosciences, 12, 4875-4894, 2015.
Lignell, R. R., Heiskanen, A.-S., Kuosa, H., Kuuppo-Leinikki, P., Pajuniemi, R., and Uitto, A.: Fate of phytoplankton spring bloom: Sedimentation and carbon flow in the planktonic food web in the northern Baltic, Marine Ecology. Progress Series, 94, 13, 1993.
Lindroth, P. and Mopper, K.: High performance liquid chromatographic determination of subpicomole amounts of amino acids by precolumn fluorescence derivatization with o-phthaldialdehyde, Analytical Chemistry, 51, 1667-1674, 1979.
Logan, B. E., Passow, U., Alldredge, A. L., Grossartt, H.-P., and Simont, M.: Rapid formation and sedimentation of large aggregates is predictable from coagulation rates (half-lives) of transparent exopolymer particles (TEP), Deep Sea Research Part II: Topical Studies in Oceanography, 42, 203-214, 1995.
Mari, X. and Burd, A.: Seasonal size spectra of transparent exopolymeric particles (TEP) in a coastal sea and comparison with those predicted using coagulation theory, Marine Ecology Progress Series, 163, 13, 1998.
Mari, X., Rassoulzadegan, F., Brussaard, C. P. D., and Wassmann, P.: Dynamics of transparent exopolymeric particles (TEP) production by Phaeocystis globosa under N- or P-limitation: a controlling factor of the retention/export balance, Harmful Algae, 4, 895-914, 2005.

Martin-Jézéquel, V., Hildebrand, M., and Brzezinski, M. A.: SILICON METABOLISM IN DIATOMS: IMPLICATIONS FOR GROWTH Journal of Phycology, 36, 821-840, 2000.
Matthäus, W. and Franck, H.: Characteristics of major Baltic inflows—a statistical analysis, Continental Shelf Research, 12, 1375-1400, 1992.
McDonnell, A. M. P., Boyd, P. W., and Buesseler, K. O.: Effects of sinking velocities and microbial respiration rates on the attenuation of particulate carbon fluxes through the mesopelagic zone, Global Biogeochemical Cycles, 29, 175-193, 2015.
Myllykangas, J. P., Jilbert, T., Jakobs, G., Rehder, G., Werner, J., and Hietanen, S.: Effects of the 2014 major Baltic inflow on methane and nitrous oxide dynamics in the water column of the central Baltic Sea, Earth Syst. Dynam., 8, 817-826, 2017.
Nausch, M., Nausch, G., Lass, H. U., Mohrholz, V., Nagel, K., Siegel, H., and Wasmund, N.: Phosphorus input by upwelling in the eastern Gotland Basin (Baltic Sea) in summer and its effects on filamentous cyanobacteria, Estuarine, Coastal and Shelf Science, 83, 434-442, 2009.
Neretin, L. N., Pohl, C., Jost, G., Leipe, T., and Pollehne, F.: Manganese cycling in the Gotland Deep, Baltic Sea, Marine Chemistry, 82, 125-143, 2003.
Passow, U.: Production of transparent exopolymer particles (TEP) by phyto- and bacterioplankton, Marine Ecology Progress Series, 236, 12, 2002.
Passow, U.: Species-specific sedimentation and sinking velocities of diatoms, Marine Biology, 108, 449-455, 1991.
Passow, U. and Alldredge, A. L.: A dye-binding assay for the spectrophotometric measurement of transparent exopolymer particles (TEP), Limnology and Oceanography, 40, 1326-1335, 1995.
Richardson, L. L., Aguilar, C., and Nealson, K. H.: Manganese oxidation in pH and O2 microenvironments produced by phytoplankton1,2, Limnology and Oceanography, 33, 352-363, 1988.
Sandberg, J., Elmgren, R., and Wulff, F.: Carbon flows in Baltic Sea food webs — a re-evaluation using a mass balance approach, Journal of Marine Systems, 25, 249-260, 2000.
Schmale, O., Krause, S., Holtermann, P., Power Guerra, N. C., and Umlauf, L.: Dense bottom gravity currents and their impact on pelagic methanotrophy at oxic/anoxic transition zones, Geophysical Research Letters, 43, 5225-5232, 2016.
Shaffer, G.: Phosphate pumps and shuttles in the Black Sea, Nature, 321, 515, 1986.
Stigebrandt, A.: Computations of oxygen fluxes through the sea surface and the net production of organic matter with application to the Baltic and adjacent seas, Limnology and Oceanography, 36, 444-454, 1991.
Strickland, J. D. and Parsons, T. R.: Determination of dissolved oxygen. In: A Practical Handbook of Seawater Analysis, Fisheries Research Board of Canada, 1968.
Strickland, J. D. H., Parsons, T. R., and Strickland, J. D. H.: A practical handbook of seawater analysis, Fisheries Research Board of Canada, Ottawa, 1972.
Thomas, H. and Schneider, B.: The seasonal cycle of carbon dioxide in Baltic Sea surface waters, Journal of Marine Systems, 22, 53-67, 1999.
Trull, T. W., Bray, S. G., Buesseler, K. O., Lamborg, C. H., Manganini, S., Moy, C., and Valdes, J.: In situ measurement of mesopelagic particle sinking rates and the control of carbon transfer to the ocean interior during the Vertical Flux in the Global Ocean (VERTIGO) voyages in the North Pacific, Deep Sea Research Part II: Topical Studies in Oceanography, 55, 1684-1695, 2008.
Turner, J. T.: Zooplankton fecal pellets, marine snow, phytodetritus and the ocean's biological pump, Progress in Oceanography, 130, 205-248, 2015.
Van Hulten, M., Middag, R., Dutay, J. C., de Baar, H., Roy-Barman, M., Gehlen, M., Tagliabue, A., and Sterl, A.: Manganese in the west Atlantic Ocean in the context of the first global ocean circulation model of manganese, Biogeosciences, 14, 1123-1152, 2017.
Van Mooy, B. A. S., Keil, R. G., and Devol, A. H.: Impact of suboxia on sinking particulate organic carbon: Enhanced carbon flux and preferential degradation of amino acids via denitrification, Geochimica et Cosmochimica Acta, 66, 457-465, 2002.

Wasmund, N.: Occurrence of cyanobacterial blooms in the baltic sea in relation to environmental conditions, Internationale Revue der gesamten Hydrobiologie und Hydrographie, 82, 169-184, 1997.
Wasmund, N. and Uhlig, S.: Phytoplankton trends in the Baltic Sea, ICES Journal of Marine Science, 60, 2003.
Wilhelm, W. L.: Die Bestimmung des im Wasser gelösten Sauerstoffes, Berichte der deutschen chemischen Gesellschaft, 21, 2843-2854, 1888.

Figure Captions

Figure 1. Monthly averaged Chl *a* distribution derived from VIIRS for June 2015 in the Baltic Sea. Black circle and "x" indicate the position of the trap deployment and the seawater collection, respectively, in Gotland Deep (GB) and Landsort Deep (LD). The lower panel shows the trajectory of the trap deployed at GB and LD.

Figure 2. Water column profiles at the location of the sediment trap deployments in (A) GB, and (B) LD. Left panel: oxygen (blue), temperature (red), and salinity (black). Middle panel: nitrate (NO_3, white squares), nitrite (NO_2, grey circles), and ammonium (NH_4, black triangles). Right panel: phosphate (PO_4, grey diamond), and silicate ($Si(OH)_4$, black circles). Grey lines indicate the depths at which we deployed sediment traps.

Figure 3. Vertical profiles of concentration of particulate organic carbon (POC), particulate nitrogen (PN), and particulate organic phosphorus (POP) in GB (A) and LD (D); vertical profiles of concentration of chlorophyll *a* (Chl *a*) and biogenic silicate (BSi) in GB (B) and LD (D); and vertical profiles of concentration of transparent exopolymeric particles (TEP) and Coomassie stainable particles (CSP) in GB (C) and LD (F) Grey lines as figure 2.

Figure 4. Vertical profiles of MnOx-like particles and O_2 concentration in the water column at the location of the sediment traps deployments. (A) GB and (B) LD. Grey lines as in figure 3.

Figure 5. Vertical fluxes of particulate organic carbon (POC) and particulate nitrogen (PN) as well as oxygen concentration in GB (A) and LD (C). Vertical fluxes of particulate organic phosphorus (POP), biogenic silica (BSi) and chlorophyll *a* (Chl *a*) in GB (B) and LD (D).

Figure 6. TEP and CSP fluxes in GB (A and B) and LD (C and D). In addition to vertical fluxes, each profile is complemented with microscopic images (200x) of material collected at each depth. In GB, star-shaped MnOx-like particles are clearly visible as single particles and forming aggregates with TEP (A), and CSP (B). MnOx-like particles were less abundant in LD (C and D). (F) A larger magnification (400x) image of MnOx-like particles at 110 m showing more detail on the shape of those particles and aggregates formed with TEP.

Figure 7. Vertical fluxes of total hydrolyzable amino acids (TAA) and total carbohydrates (TCHO) as well as oxygen concentration in (A) GB, and (B) LD.

Table 1. Sediment traps deployment and recovery locations, dates, collection times and depths.Two sediment traps were deployed at 40 m (A and B) to evaluate replicability.

Station	Lat	Lon	Date	Station depth	Deployment time (d)	Trap depths (m)
Gotland Basin (GB)	57.21 °N	20.03 °E	08/06/2015	248 m	2	40A, 40B, 60, 110, and 180m
	57.27 °N	20.25 °E	10/06/2015			
Landsort Deep (LD)	58.69 °N	18.55 °E	15/06/2015	460 m	1	40A, 40B, 55, 110, and 180m
	58.68 °N	18.68 °E	16/06/2015			

Table 2. Abundance of chlorophyll and phycoerythrin containing pico- and nano-plankton measured by flow cytometry in GB and LD.

		Phytoplankton (cells mL^{-1})			Cyanobacteria-like (cells mL^{-1})		
	Depth (m)	picoplankton	nanoplankton	Total	picoplankton	nanoplankton	Total
GB	1	87963	2097	90060	5225	731	5956
	10	94369	2628	96997	8795	920	9716
	40	4999	68	5067	2174	69	2243
	60	4125	35	4160	1990	42	2032
	80	599	7	606	238	15	253
	110	594	7	601	326	29	356
	140	1144	14	1158	356	2	358
	180	908	9	917	366	20	385
	220	2270	19	2289	1063	34	1097
LD	1	92359	2283	94642	834	177	1011
	10	86426	1708	88134	2990	232	3223
	40	2022	92	2114	2243	69	2312
	60	1524	62	1586	1294	24	1318
	70	908	43	951	613	17	630
	110	1735	82	1817	1181	17	1198
	180	1339	75	1415	946	34	980
	250	1593	82	1676	949	36	985
	300	1521	48	1569	1047	17	1064
	350	1608	57	1665	908	12	920
	400	1548	73	1621	1047	22	1069
	430	1562	68	1631	875	19	894

Table 3. Phytoplankton abundance analyzed microscopically for samples collected at the location of trap deployment in GB and LD.

		Phytoplankton Abundance (L^{-1})							
		GB				LD			
		1 m	10 m	40 m	Total	1 m	10 m	40 m	Total
Cyanobacteria*	Total	14148	13536	0	27684	37368	32526	96	69990
Chryptophyta	Total	140	112	28	280	1400	882	56	2338
Bacillariophyceae	Total	96	94	44	234	462	112	102	676
	Chaetoceros sp.	58	42	24	124	434	106	26	566
	Skeletonema sp.	26	8	12	46	12	0	8	20
	Thalassiosira sp.	12	44	8	64	16	6	68	90
Dinophyceae**	Total	3772	4424	1192	9388	9032	7662	1404	18098
	Dinophysis sp.	678	742	2	1422	450	214	4	668
	other	3094	3682	1190	7966	8582	7448	1400	17430
Chlorophyta	Total	5320	6860	28	12208	2072	1022	238	3332
	Planctonema sp.	5320	6860	28	12208	2072	1022	238	3332

*Filamentous cyanobacteria were counted in 50 µm length units (>90% were *Aphanizomenon* sp.)

**Include mixotrophs

Table 4. MnOx-like particle fluxes and size as equivalent spherical diameter (ESD) determined by image analysis in GB and LD.

Station	Depth (m)	MnOx-like particles (cm^2 $m^{-2}d^{-1}$)	Median size ESD (μm)	Size range ESD (μm)
GB	110	5666± 994	2.8	0.6-167
	180	7789± 955	3.3	0.6-153
LD	110	50.3±1.8	1.8	0.6-16.5
	180	2.6±0.3	1.4	1.2-9.3

Table 5. Amino acids (AA), carbohydrates (CHO), elemental molar ratios and amino acid-based degradation index of sinking and suspended particles in GB and in LD.

		Depth (m)	AA-C:POC %	CHO-C:POC %	POC:PN	POC:POP	POC:BSi	PN:BSi	PN:POP	DI
Sinking particles	GB	40	19.2	18.3	9.8	244	3.9	0.4	24.9	1.49
		40	17.6	17.2	9.4	222	4.1	0.4	23.6	1.43
		60	15.8	17.6	9.5	232	2.8	0.3	24.3	1.13
		110	13.9	22.2	11.3	90.1	1.7	0.2	8.0	0.71
		180	11.1	18.5	12.7	123	3.0	0.2	9.7	-0.03
	LD	40	13.5	9.4	12.2	772	3.6	0.3	63.4	0.30
		40	14.3	8.4	11.1	413	4.1	0.4	37.2	0.27
		55	19.1	11.0	12.4	332	3.0	0.2	26.7	-0.02
		110	13.4	12.0	15.4	230	2.7	0.2	14.9	0.11
		180	14.3	12.9	15.3	341	4.2	0.3	22.3	-0.29
Suspended particles	GB	1	8.2	16.9	10.4	155	91.4	8.8	14.9	
		10	10.8	8.8	10.5	151	87.1	8.3	14.4	
		40	4.9	2.8	9.2	88.8	134	15	9.7	-0.81
		60	5.4	2.7	9.8	127	125	13	13.0	-0.27
		80	4.7	0.00	10.4	145			13.9	
		110	9.0	6.6	8.5	245			29.0	0.98
		140	5.3	0.00	10.6	283			26.7	
		180	5.7	4.3	11.4	506			44.5	-0.40
		220	8.6	3.3	12.1	271			22.5	
	LD	1	7.0	0.00	8.7	205	515	59.5	23.7	
		10	13.0	9.1	8.4	196	101	12.0	23.3	
		40	0.00	8.9	8.1	336	24.5	3.0	41.5	-0.53
		60	6.1	10.3	7.8	301	16.9	2.2	38.4	-0.12
		70	7.9	10.7	7.7	292	248	32.1	37.9	
		110	12.2	5.4	7.9	225			28.3	0.80

	180	10.1	11.3	7.0	205	29.2	0.34
	250	12.0	8.8	6.5	249	38.2	
	300	10.9	0.00	6.7	137	20.4	
	350	10.7	10.1	6.8	146	21.6	
	400	10.0	0.00	6.2	230	37.2	
	430	9.4	9.5	7.8	149	19.0	

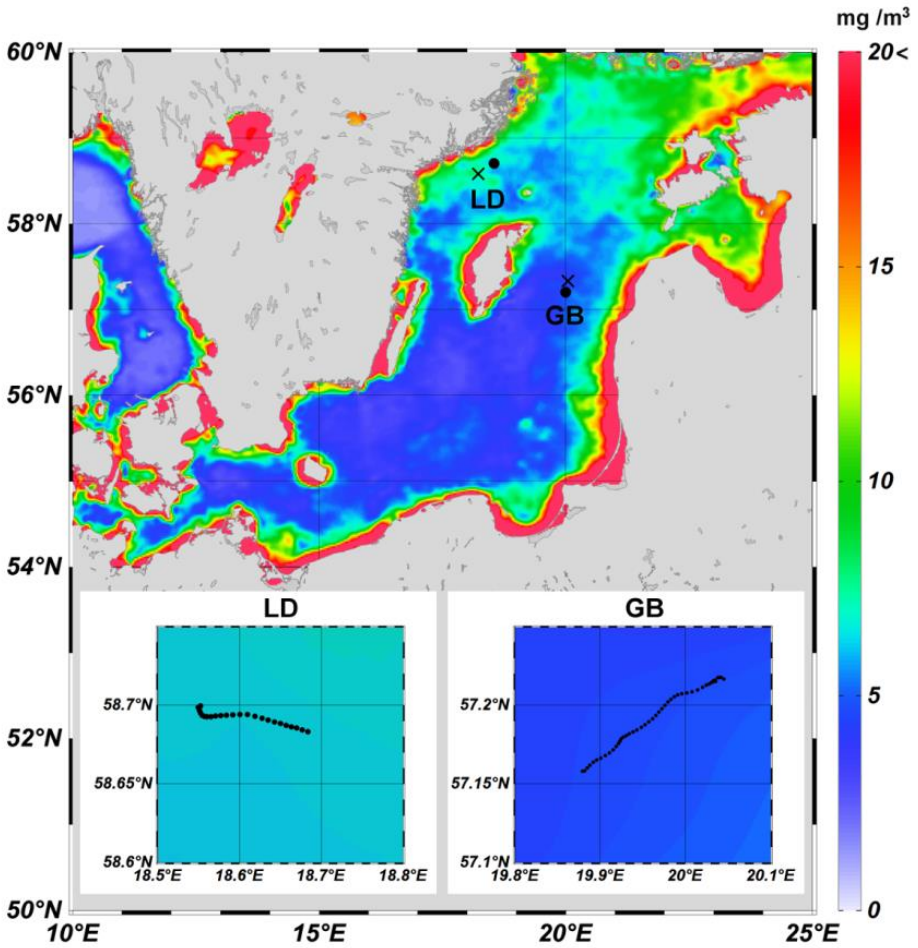
mg /m³
20<
15
10
5
0
60°N
58°N
56°N
54°N
52°N
50°N
10°E
15°E
20°E
25°E
LD
GB
LD
58.7°N
58.65°N
58.6°N
18.5°E
18.6°E
18.7°E
18.8°E
GB
57.2°N
57.15°N
57.1°N
19.8°E
19.9°E
20°E
20.1°E

Fig. 1

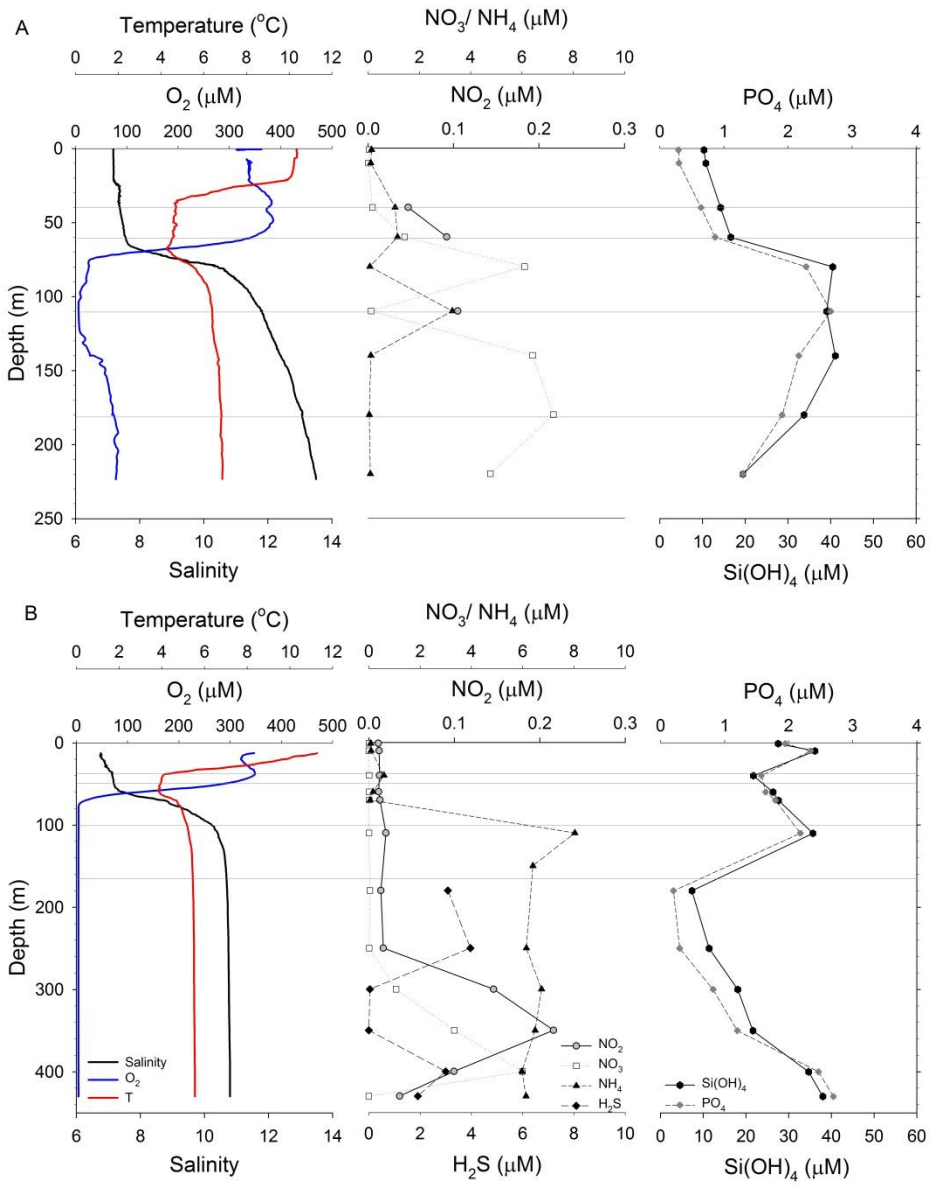
A
Temperature (°C)
NO_3/ NH_4 (µM)
O_2 (µM)
NO_2 (µM)
PO_4 (µM)
Depth (m)
Salinity
$Si(OH)_4$ (µM)
B
Temperature (°C)
NO_3/ NH_4 (µM)
O_2 (µM)
NO_2 (µM)
PO_4 (µM)
Depth (m)
Salinity
O_2
T
NO_2
NO_3
NH_4
H_2S
$Si(OH)_4$
PO_4
Salinity
H_2S (µM)
$Si(OH)_4$ (µM)

Fig. 2

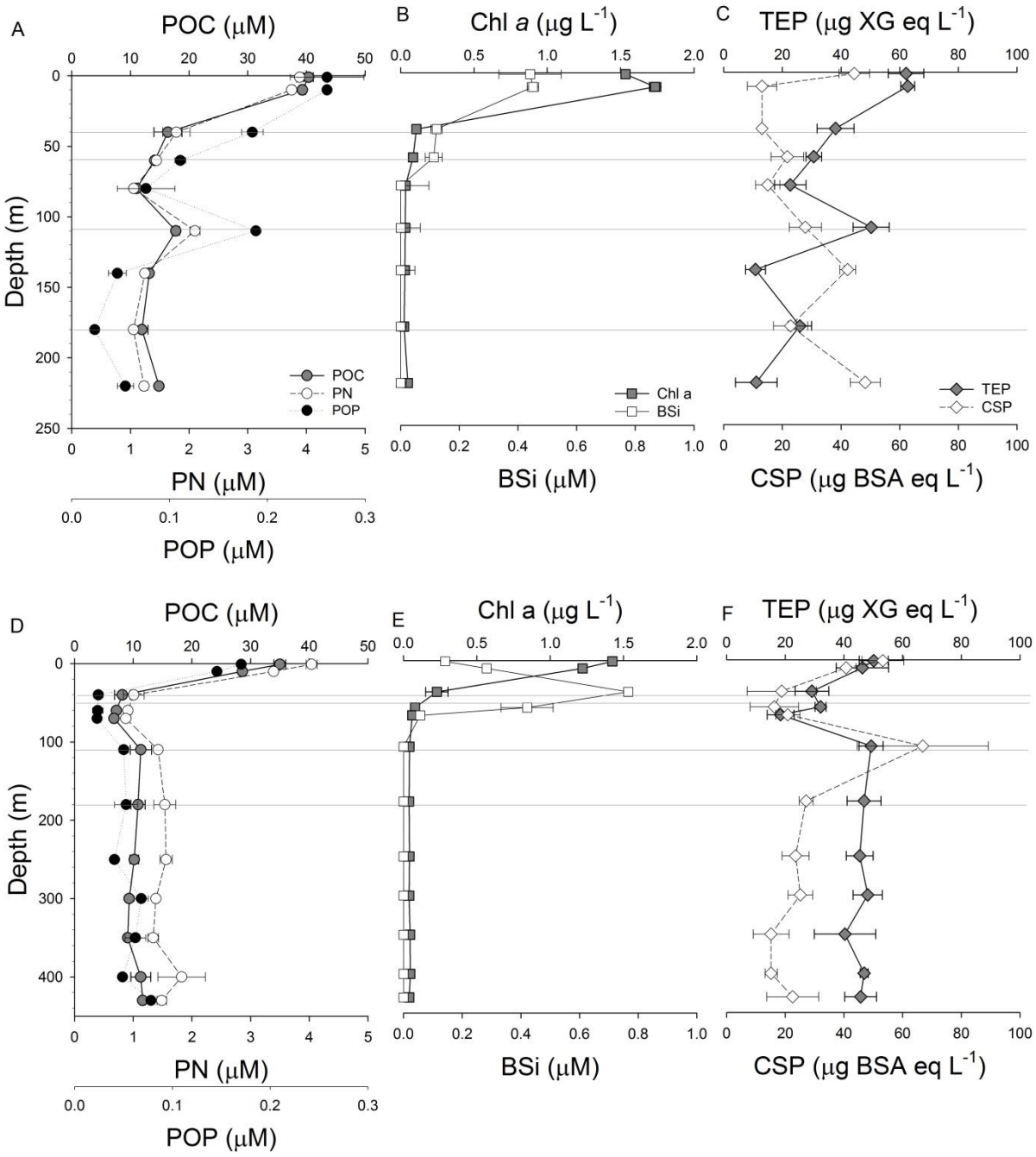
A
POC (μM)
Depth (m)
POC
PN
POP
PN (μM)
POP (μM)
B
Chl a (μg L-1)
Chl a
BSi
BSi (μM)
C
TEP (μg XG eq L-1)
TEP
CSP
CSP (μg BSA eq L-1)
D
POC (μM)
Depth (m)
PN (μM)
POP (μM)
E
Chl a (μg L-1)
BSi (μM)
F
TEP (μg XG eq L-1)
CSP (μg BSA eq L-1)

Fig. 3

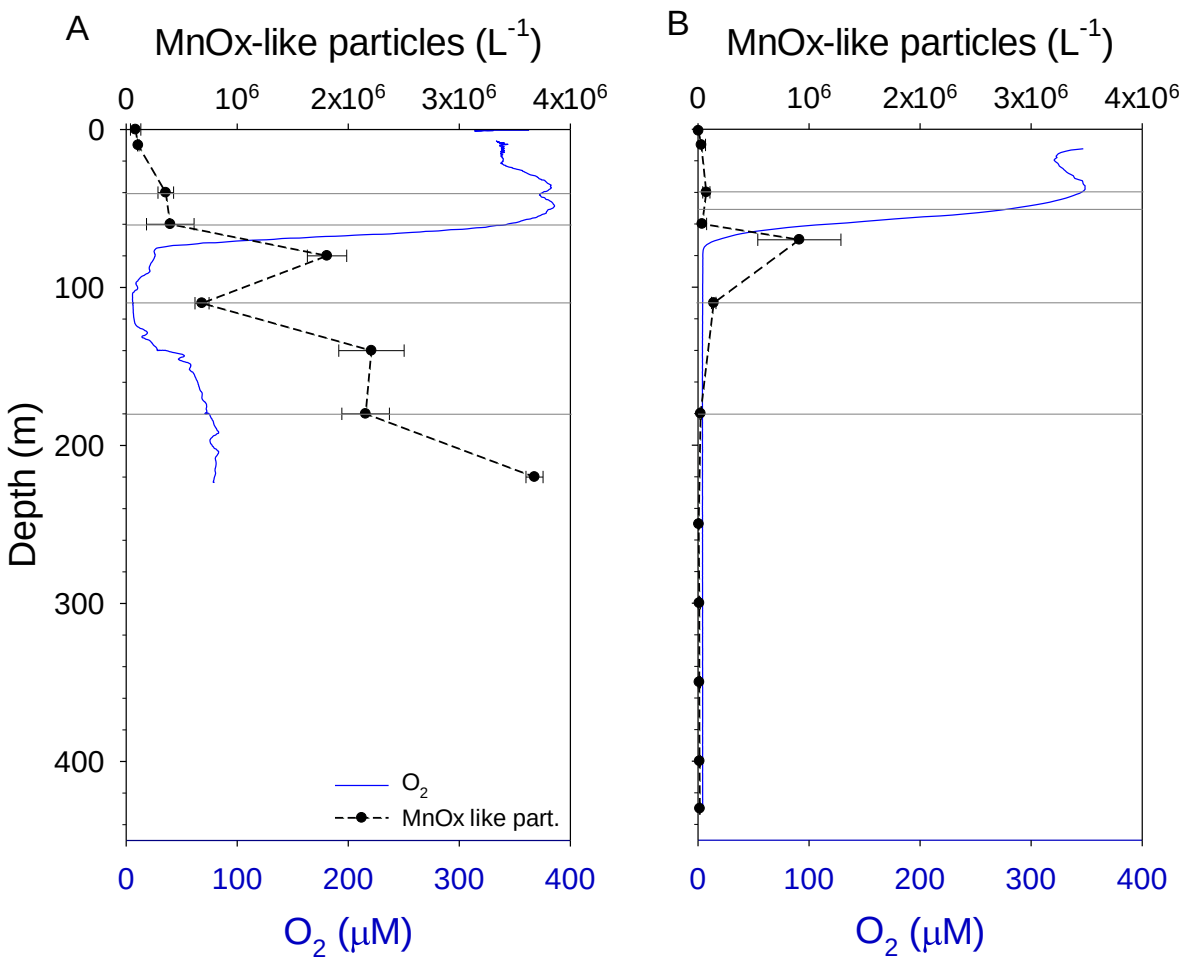
A
MnOx-like particles (L-1)
0
10^6
2x10^6
3x10^6
4x10^6
Depth (m)
0
100
200
300
400
O2
MnOx like part.
O2 (µM)
B
MnOx-like particles (L-1)
O2 (µM)

Fig. 4

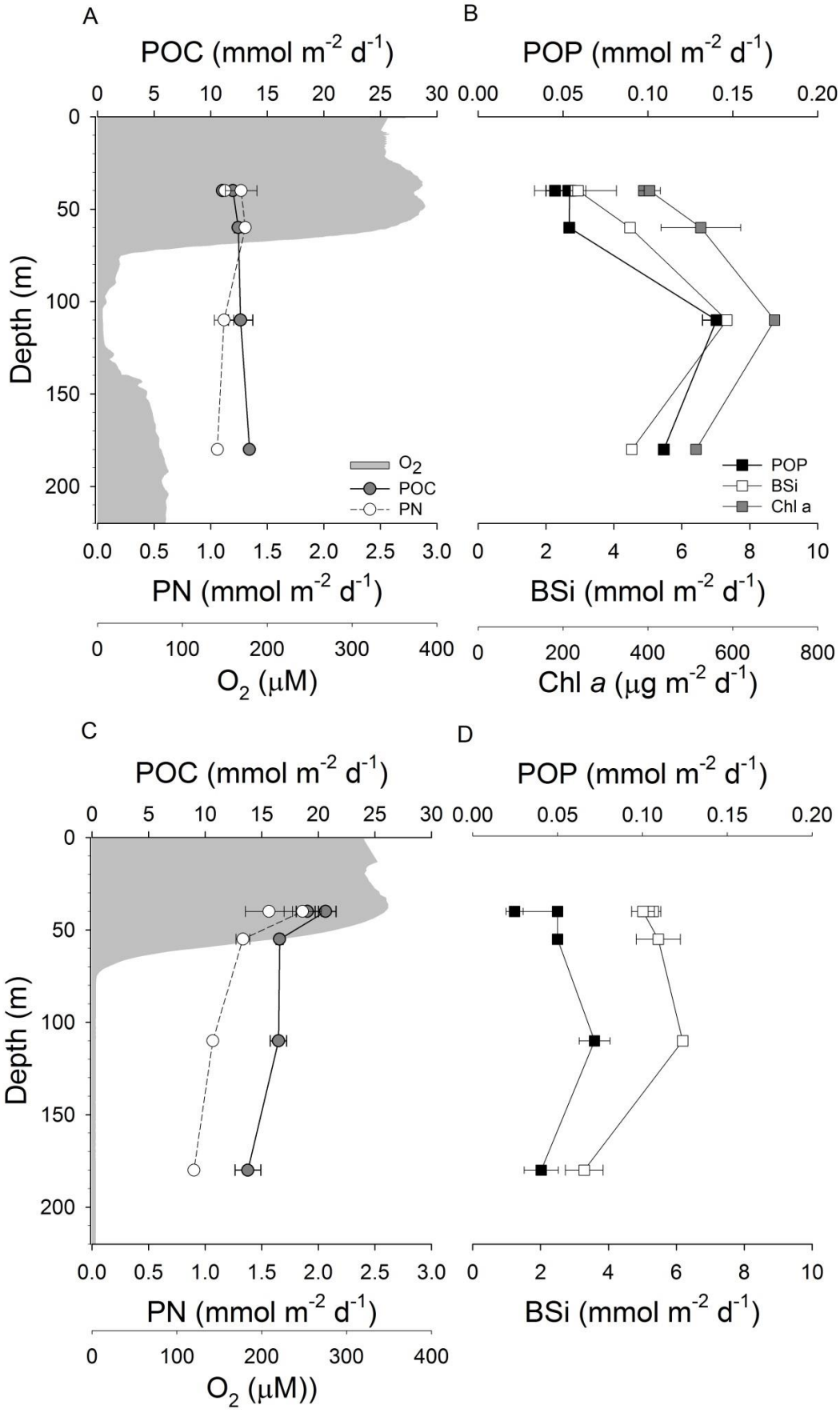
A
POC (mmol m-2 d-1)
0 5 10 15 20 25 30
B
POP (mmol m-2 d-1)
0.00 0.05 0.10 0.15 0.20
Depth (m)
0 50 100 150 200
O2
POC
PN
POP
BSi
Chl a
0.0 0.5 1.0 1.5 2.0 2.5 3.0
PN (mmol m-2 d-1)
0 2 4 6 8 10
BSi (mmol m-2 d-1)
0 100 200 300 400
O2 (µM)
0 200 400 600 800
Chl a (µg m-2 d-1)
C
POC (mmol m-2 d-1)
D
POP (mmol m-2 d-1)
Depth (m)
PN (mmol m-2 d-1)
BSi (mmol m-2 d-1)
O2 (µM))

Fig. 5

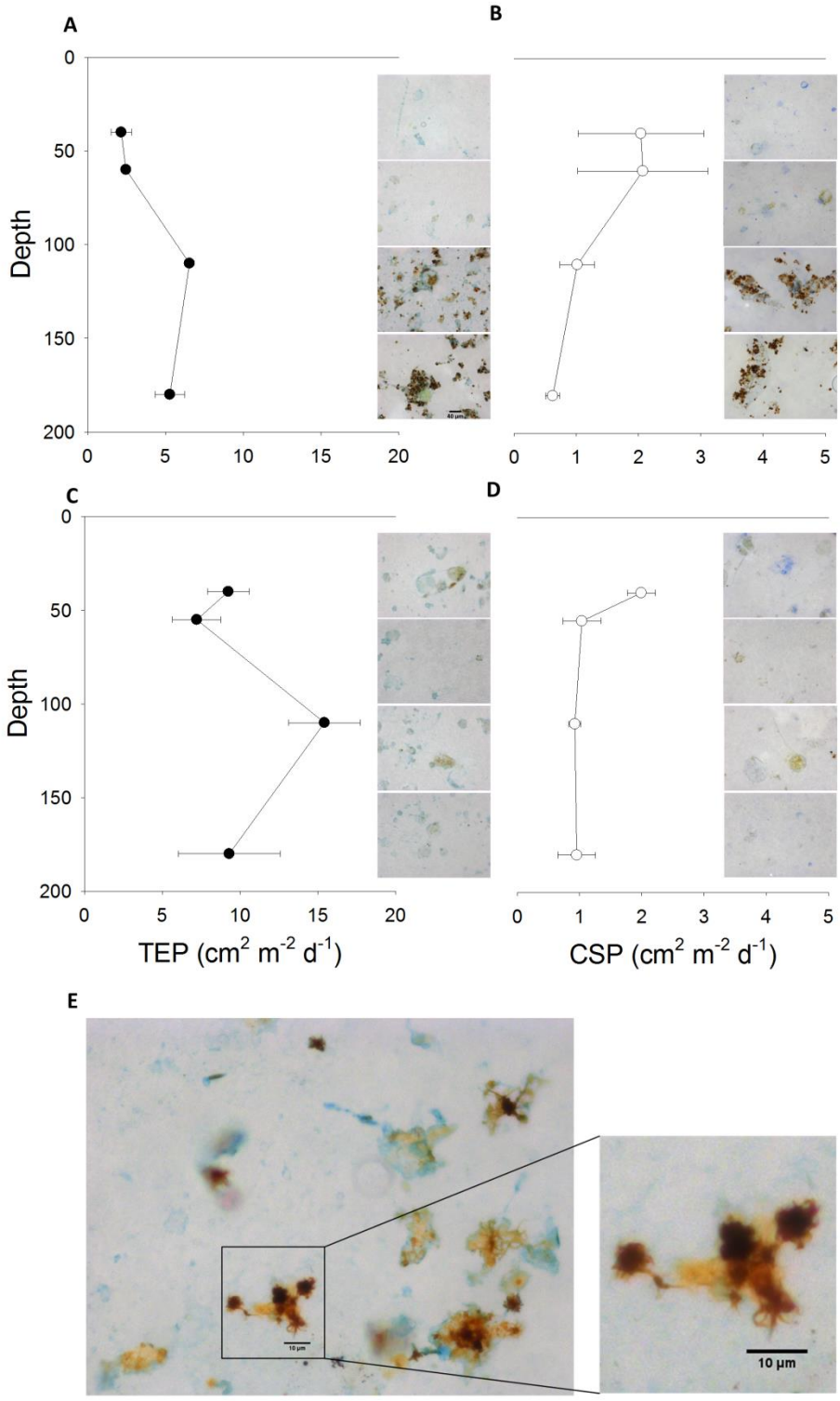
A
B
C
D
E
Depth
0
50
100
150
200
0
5
10
15
20
1
2
3
4
TEP (cm^2 m^{-2} d^{-1})
CSP (cm^2 m^{-2} d^{-1})
10 µm

Fig. 6

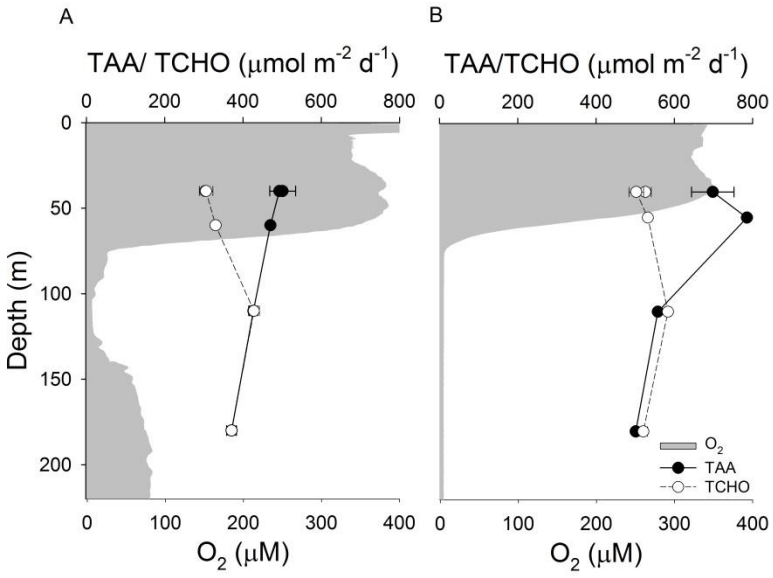
A
B
TAA/ TCHO (μmol m-2 d-1)
TAA/TCHO (μmol m-2 d-1)
0
200
400
600
800
Depth (m)
0
50
100
150
200
0
100
200
300
400
O2 (μM)
O2
TAA
TCHO

Fig. 7